Vortex Scattering In Bose-Einstein Condensates

Adam Griffin

Supervisors:

Prof N. Proukakis

Prof C. Barenghi

1^{st} May 2015

Abstract

We present a numerical study of the dynamics of the 'quantum vortex' via simulations of the Gross-Pitaevskii equation. We first discuss the well researched single vortex case and the interactions of two quantum vortices of equal and or opposite sign. We then begin to develop an understanding of a particular interaction of three quantum vortices. The interaction in question is that of a vortex pair incident on a single vortex. This aim is to investigate whether the interaction can be characterized by the scattering angle of the vortex pair. This case is of experimental relevance and not yet been investigated in this way to the best of our knowledge. To best visualize results we present videos of the simulations referenced throughout.

Contents

Chapter 1

Introduction

1.1 Vortices In Nature

The term vortex describes rotational motion in fluids. Such motions arise in an abundance of systems in nature, extreme examples being hurricanes [1] and volcano smoke rings [2] with more everyday examples including insect flight [3] and blood flow [4]. Considering such a vast range of areas in which this motion plays an integral role in a systems dynamics, it is no wonder that it is such a popular and fruitful field of research. The concept of a vortex is well known, however it is harder to specify a precise mathematical definition due to the differing motions involved in a single vortex. Take, for example, the definition given by Saffman and Baker [5] which states:
"A vortex is a finite volume of rotational fluid, bounded by irrotational fluid or solid walls".
By this definition the vortex is not only defined by the rotational elements of the system but rather by the contrast in motions of a fluid. This idea is key when describing a vortex, as a vortex is described by the entire system it is contained in and not just the singularity at the axis of which it rotates.

The quantum world hosts its own version of the vortex which, as with most things quantum, has peculiar properties. These types of vortices, dubbed "quantum vortices", are particularly interesting due to them arising in quantized form. Flows which contain quantum vortices or exhibit quantum behavior, such as lack of viscosity, are often called quantum fluids. Examples of such fluids are liquid helium and electrons within superconductors, both of which are believed to be different manifestations of a single physical system. The system is the Bose-Einstein condensate and is the medium in which we shall study quantum vortices.

1.2 The Bose-Einstein condensate

Particles in nature appear in two types: bosons and fermions. The difference between these types of particle is the spin. Spin is to be thought of as a particles angular mo-

mentum around its own axis, although this is just an analogy, the mathematical laws followed by spin are the same as the laws followed by quantized angular momentum. Bosons have integer spin whereas fermions have half integer spin. A consequence of fermions having half integer spin is Pauli's exclusion principle. This principle states that no two fermions can occupy the same energy state. Bose-Einstein condensation is a phenomenon in which many bosons occupy the lowest energy state in a system. Although it is possible for pairs of fermions to undergo Bose-Einstein condensation in certain scenarios, such as so-called Cooper pairs, the focus of this report is solely on bosons, which unlike fermions are free to share energy states.

Bose-Einstein condensation was first predicted by Satyendra Nath Bose in 1924. Bose was a self taught Indian physicist who was unknown to the scientific community. Being unknown he struggled to publish his results and so he contacted Einstein for help. Einstein was impressed by the work of Bose and submitted it on behalf of him. Bose's work focused on photons and suggested that it was incorrect to treat two photons of equal energy as distinct and identifiable. Einstein generalized Bose's work by applying the same idea to atoms. Einstein's work focused on a gas of noninteracting atoms; within this framework he had predicted a so-called phase transition associated with atoms condensing into the lowest energy state. A good description of this condensation is found by considering the de-Broglie wave length of an atom. It is well established in physics that atoms behave like waves and that the de-Broglie wavelength of a particle with momentum p is given by $\lambda = h/p$, where h is Planck's constant. Using this formula for a system in which most atoms are approaching the lowest energy state, thus having low momentum, it is clear that the de-Broglie wavelength will become larger. Eventually the wavelength of each individual atom will become large enough that the individual atoms' wavelengths occupy the same momentum space as numerous other atoms, therefore making the atoms indistinguishable.

The first pure Bose Einstein condensate was not created until 1995 when two groups independently created a condensate. One group was at JILA [6] with a team including Carl Wieman and Eric Cornell and another was lead by Wolfgang Ketterle [7] at MIT. The three mentioned received the 2001 physics Nobel prize for their efforts. The reason why it took over 70 years since its prediction to create a 'clean' condensate was due to the difficulty of cooling a gas to temperatures low enough to witness the phase transition without the particles forming a solid. To solve this problem experimentalists engineered a new way to cool down atoms called laser cooling. The idea is to bombard an atom with photons from all directions to slow it in each direction, this is analogous to bombarding a moving jumbo jet with millions of ping pong balls to eventually halt its motion. This technique cooled the atoms down to an astonishingly low temperature but was still not enough to realize the condensate. To cool the atoms even further a new idea was implemented. The idea was to use evaporative cooling. The method of evaporative cooling consists of using a magnetic field to trap atoms. The magnetic field is non-homogeneous, therefore there will not be an even distribution of energy between atoms. The final stage of the cooling is to decrease the magnetic field trapping the atoms

so that only the highest energy atoms can escape. This decreases the average kinetic energy of a particle in the system, which is equivalent to a temperature decrease. This is much like how a cup of tea cools, the particles with highest energy on the surface take energy from the system thus cooling it. Applying both these ideas the condensate was created. Since then many have been created all over the world and the study both experimentally and theoretically has become a major field in science.

1.3 Quantum Vortices

Lars Onsager [8] was first to make note of quantized vortices in the context of superfluidity which has deep links with Bose-Einstein condensation. He noted that the circulation of vortices in superfluids are quantized. Onsager rather humbly announced this in the footer of a paper and did not provide any details or reasoning. Even with the lack of details the consequence for science was enormous, with Russell Donnelly [9] suggesting that the ratio of scientific insight to length of announcement must be the highest in history. This work was more formally described by Richard Feynman [10] in 1955. The theoretical results derived by Onsager and Feynman were tested by Hall and Vinen [11] in 1956 and were shown to match the experimental data. Quantum vortices have been witnessed in Bose-Einstein condensates [12]. Experimental ingenuity has produced vortices in BECs with many methods now able to create and study these structures. The methods include rotating the condensate and witnessing the creation of vortices which then proceed to form grid-like formations which are known as vortex lattices [13], others include moving a laser through the condensate with vortices forming in the laser's wake [14] as shown in figure 1.1. A single quantum vortex in an infinite plane is stable, whereas two vortices have interesting but simple interactions. When the configuration holds three vortices the motions become more complex and a system containing four or more vortices can be shown to be chaotic [15].

Within this report we shall discuss two models for quantum vortices; the classical point vortex of the inviscid Euler fluid, mainly for a comparison tool, and the Gross-Pitaevskii equation which is a model of the zero-temperature Bose-Einstein condensate. We then proceed by simulating the Gross-Pitaevskii equation, firstly in one dimension followed by a study of vortices in two dimensions. The final section of the report is focused on characterizing a particular interaction of three vortices. Although there have been studies which investigate similar interactions [16], we have not found any papers that particularly focus on the scattering angle.

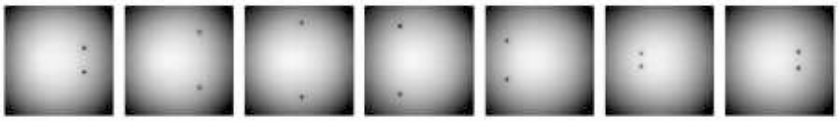

Figure 1.1: Image of vortex-antivortex pair created by moving laser through a condensate confined to a harmonic trap taken from [14].

Chapter 2

Vortex Models

2.1 Classical Vortices

The first model we shall discuss is the point vortex model within the framework of the incompressible, inviscid Euler fluid. The Euler fluid is highly idealized however it is in fact a good approximation for many real systems and relevant for weakly-interacting gases which lack viscosity. Recall the incompressible Euler equations for a fluid with a velocity field $\mathbf{v}$, constant density ρ and pressure p;

$$\nabla \cdot \mathbf{v} = 0, \tag{2.1}$$

$$\frac{\partial \mathbf{v}}{\partial t} + (\mathbf{v} \cdot \nabla)\,\mathbf{v} + \frac{1}{\rho}\nabla p = 0. \tag{2.2}$$

Equation (2.1) represents the incompressibility condition of the fluid and Equation (2.2) describes an ideal fluid's motion. The study of vortices requires a measure of rotation of fluid. The measure is called the vorticity and is given by

$$\boldsymbol{\omega} = \nabla \times \mathbf{v}, \tag{2.3}$$

which describes how an object would tend to rotate in a fluid at a particular point. Taking the divergence of (2.3) gives the condition

$$\nabla \cdot \boldsymbol{\omega} = 0. \tag{2.4}$$

An important property of a fluid with respect to vortices is the circulation. The circulation is given by the equation

$$\Gamma = \oint_{\mathcal{L}} \mathbf{v} \cdot d\mathcal{L}, \tag{2.5}$$

where $\mathcal{L}$ is a closed contour. The circulation is a measure of the rotation of the fluid on the contour of the line integral and can be shown [17] to be conserved by Kelvin's theorem. It is conventional to define a vortex with circulation around the core in a anti-clockwise direction to be a vortex and circulation in the opposing direction to be

an antivortex. The focus of this report is the interaction of vortices, it can be shown [9] that for two hollow vortices contained in a two dimensional fluid of inside a region of diameter b, density ρ, empty cores with diameters a and a separation of d, the energy per unit length is given by

$$K_R = \left(\frac{\rho\Gamma^2}{2\pi}\right)\ln\left(\frac{b^2}{ad}\right) \quad \text{or} \quad K_P = \left(\frac{\rho\Gamma^2}{2\pi}\right)\ln\left(\frac{d}{a}\right) \tag{2.6}$$

depending on the circulation of the vortices. K_R is the energy when the vortices have equal circulation and rotate around one another. K_P represents the energy when the circulations are of equal magnitude but are of opposite sign which is the system in which the cores move in a in a parallel motion also known as a vortex-antivortex pair. The speed and angular speed for each respective configuration can be found if we neglect any effects of the core and are given by

$$v_P = \frac{\Gamma}{2\pi d}. \tag{2.7}$$

$$\omega_R = \frac{\Gamma}{\pi d^2} \tag{2.8}$$

Neglecting the core makes the vortices effectively point vortices, that is, fluid rotating around an infinitesimal singularity. A schematic is given in figure 2.1.

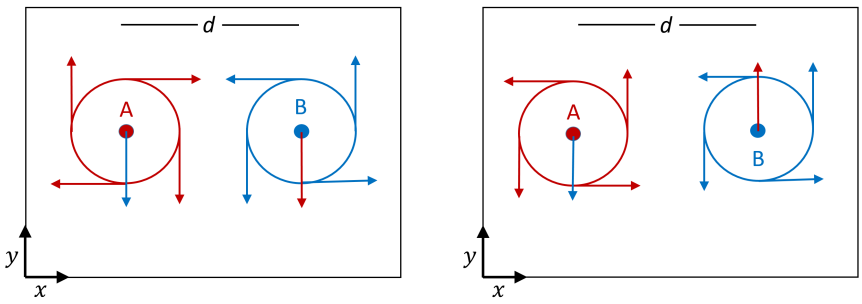

(a) (b)

Figure 2.1: Two dimensional vortex schematics: The red arrows correspond to the contribution of vortex A to the velocity field where the blue arrows correspond to vortex B. The filled circles correspond to the singularity at the center of the vortex which are separated by a distance d. (a) represents vortices with equal magnitude in opposite directions where A can be considered an antivortex and (b) represents vortices with equal circulation in both magnitude and direction.

As you can see in figure 2.1a, the contributions to the velocity field from both vortex A and vortex B push the opposing vortex in the negative y-direction. The resulting velocity field will cause motion of the vortex singularities in the negative y-direction with a velocity v_p given from equation (2.7). The motion involved in 2.1b takes a little more imagination. The initial velocity field is pushing the vortices singularities in opposing

directions; however after the vortices begin to move the velocity field contributions from each vortex will also move. The resulting motion will be a rotation of both vortices around the midpoint between them. The vortices will rotate at angular speed ω_R. There are not many systems in which actual two dimensional vortices exist; however, they can be a good approximation for three dimensional systems. Take for example a hurricane on earth. The earths atmosphere is around 10km thick, this compared with the earths surface is negligible. On large scales the hurricane would appear two dimensional. In a similar sense the motions of a vortex-antivortex pair can be viewed as a two dimensional approximation to a three dimensional vortex ring as shown in figure 2.2. By taking a slice of the vortex ring the effects from the z-direction are being neglected.

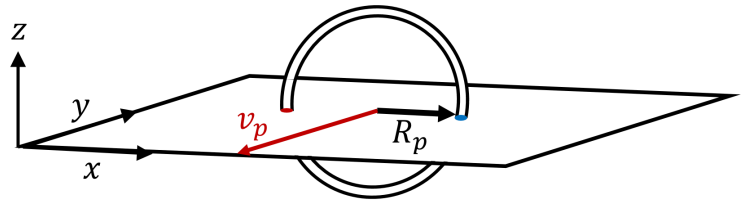

Figure 2.2: Vortex ring: This figure shows how a vortex ring can be viewed in 2D. The trapezoid shows a 2 dimensional box where intersections with the ring are vortices shown as red dots, in two dimensions this box would look exactly like 2.1a. The vortex ring's speed can be approximated as v_p depending on the radius which is the equivalent to half the separation, d, in two dimensions. Although there are better models for vortex rings, for small cores compared to the radius the approximation is reasonable.

2.2 Background of Quantum Mechanics

Before the end of the 19th century physics was largely described by deterministic mathematics on the basis of macroscopic quantities. The increase in abilities to experiment opened up the microscopic world. The classical models failed to describe many experiments and so the formulation of quantum mechanics began. Through this new theory the wave function was born. The wave function describes a particle in a quantum system and how it changes with respect to space and time. Unlike classical mechanics a particle is represented by a wave (hence 'wave' function), where the most common way to interpret the wave function is through the relation $|\Psi(\mathbf{r},t)|^2 = Pr(\mathbf{r},t)$, where $Pr(\mathbf{r},t)$ is the probability of a particle being in position $\mathbf{r}$ at time t. This relation implies that the normalization condition hold as it would be unrealistic to have probabilities that did not sum to one, that is,

$$\int |\Psi(\mathbf{r},t)|^2 \, d\mathbf{r} = 1. \tag{2.9}$$

For systems of more than one particle the wave function can be interpreted to represent number density through the relation $|\Psi(\mathbf{r},t)|^2 = n(\mathbf{r},t)$, where $n(\mathbf{r},t)$ is the particle density of a particles in position $\mathbf{r}$ at time t. This then implies the normalization condition,

$$\int |\Psi(\mathbf{r},t)|^2 \, d\mathbf{r} = N, \tag{2.10}$$

where N is the total number of particles. The wave function is a solution to Schroedinger's equation,

$$i\hbar \frac{\partial \Psi(\mathbf{r},t)}{\partial t} = \hat{H}\Psi(\mathbf{r},t), \tag{2.11}$$

where $\hat{H}$ is a Hamiltonian which describes the energy of the system and $\hbar = h/2\pi$ is Planck's reduced constant which is associated with the quantization of energy. The form of the Schroedinger equation for a non-interacting ideal particle is,

$$i\hbar \frac{\partial \Psi(\mathbf{r},t)}{\partial t} = \left(\frac{-\hbar^2}{2m}\nabla^2 + V_{ext}(\mathbf{r}) \right) \Psi(\mathbf{r},t). \tag{2.12}$$

In the equation above V_{ext} is the trapping potential and m the mass of the particle. This form of the Schroedinger equation is specifying a system where only two forms of energy are present, that is kinetic in the first term on the right hand side, and external potential given by the second term on the right hand side.

2.3 The Gross-Pitaveskii Equation

The Gross Pitaevskii equation, derived independently by Eugene Gross [18] and Lev Pitaevskii [19] in 1961, describes a BEC formed in a weakly interacting dilute Bose gas at zero temperature. A weakly interacting Bose gas is a dilute gas of bosons which obeys Bose-Einstein statistics. The weakly interacting Bose gas has the following properties. The first property is that three or more body collisions are rare and can be safely neglected when mathematically describing the gas. Another property of the weakly interacting bosonic gas is that the range of interatomic forces is much smaller than the average distance between particles. The average distance between particles for a gas of N particles in a volume V is $d = n^{-1/3}$ where n is the number density fixed by the relation $n = N/V$. For a weakly interacting Bose gas confined via an external potential V_{ext} it can be shown [20] that under the certain approximations one can derive the Gross-Pitaevskii equation,

$$i\hbar \frac{\partial}{\partial t}\Psi(\mathbf{r},t) = \left(-\frac{\hbar^2\nabla^2}{2m} + V_{ext}(\mathbf{r}) + g|\Psi(\mathbf{r},t)|^2 \right) \Psi(\mathbf{r},t). \tag{2.13}$$

where g, the magnitude of the energy exchange of an approximate 'snooker ball' type collision, is given by

$$g = \frac{4\pi\hbar^2 a}{m}, \tag{2.14}$$

for the scattering length a which characterizes the repulsive interaction between the bosons. The number of particles within the system is conserved,

$$\int |\Psi(\mathbf{r},t)|^2 d\mathbf{r} = N. \tag{2.15}$$

then trivially total mass $\mathcal{M}$,

$$m \int |\Psi(\mathbf{r},t)|^2 d\mathbf{r} = \mathcal{M} \tag{2.16}$$

where m is the mass of a single particle. It can also be shown that the energy is conserved in the system and can be described using the following integral,

$$E = \int \left[\frac{\hbar^2}{2m} |\nabla\Psi|^2 + V_{ext} |\Psi|^2 + \frac{g}{2} |\nabla\Psi|^4 \right] d\mathbf{r}. \tag{2.17}$$

The expression for the energy describes the kinetic energy in the system via the term $(\hbar^2/2m)|\nabla\Psi|^2$, the potential energy by $V_{ext}|\nabla\Psi|^2$ and the interaction energy by $(g/2)|\Psi|^4$. The equation (2.13) is a generalized form of Schroedinger's equation (2.11) and is often referred to as the non-linear Schroedinger equation. The difference is the extra term which describes interactions of particles which comes from the two-body Hamiltonian. It is useful to consider steady solutions to this equation, that is solutions independent of time. The time independent Gross-Pitaevskii equation can be found by considering the evolution of the state,

$$\Psi(\mathbf{r},t) = \psi(\mathbf{r}) e^{-\frac{i\mu t}{\hbar}}. \tag{2.18}$$

μ is the chemical potential of a boson which represents the change in ground state energy when one boson is added to the system. Applying this substitution to equation (2.13) we find

$$\mu\psi = \left(-\frac{\hbar^2\nabla^2}{2m} + V_{ext}(\mathbf{r},t) + g|\psi|^2 \right) \psi. \tag{2.19}$$

The Gross-Pitaevskii equation provides an excellent tool for studying large scale behavior of Bose-Einstein condensation but due to the approximations applied it is not valid for microscopic scales.

2.4 Analytical Solutions

2.4.1 Uniform Solution

To find a steady solution we consider the time independent Gross-Pitaevskii Equation and for a uniform density which implies $\frac{\partial^2\psi}{\partial x^2} = 0$ and no external potential, $V_{ext} = 0$, then the time independent GP equation (2.19) becomes,

$$g|\psi|^2\psi = \mu\psi. \tag{2.20}$$

By rearranging, the solution in one dimension is given by,

$$\psi(x) = \psi_0 = \sqrt{\frac{\mu}{g}}. \tag{2.21}$$

It is simpler to write this in terms of the real valued density,

$$n(x) = n_0 = \psi_0^2 = \frac{\mu}{g}. \tag{2.22}$$

The density and wave function are constant in an infinite sized system with no external potential. This shows that the chemical potential, interaction strength and density are trivially linked as you would expect. A system with conserved number density with a higher chemical potential will have a higher interaction strength.

2.4.2 Semi-Infinite Trap

Consider an infinite one dimensional plane with a potential defined as,

$$V(x) = \infty \text{ when } x < 0 \qquad V(x) = 0 \text{ when } x \geq 0 \tag{2.23}$$

This setup is called the semi-infinite trap because no particle can be in the region $x < 0$ as it would require infinite energy. This setup has two constraints,

$$\psi(0) = 0 \qquad \psi(x) = \psi_0 = \sqrt{\frac{\mu}{g}} \text{ as } x \to \infty, \tag{2.24}$$

where the first of the constraints in (2.24) is a consequence of the infinite energy at $x = 0$ and the second is due to the limiting case where the wave function will not interact with the boundary the wave function is required to become the solution in an infinite plane as in (2.22). To find a steady solution we once again consider the time independent Gross-Pitaevskii equation in the region of zero external potential. Applying these conditions to equation (2.19), one arrives at,

$$\mu\psi = \left(-\frac{\hbar^2}{2m}\frac{\partial^2}{\partial x^2} + g|\psi|^2\right)\psi. \tag{2.25}$$

Now using the second constraint we rearrange to find $\mu = \psi_0^2 g$, substituting this into the above equation gives

$$\frac{\partial^2\psi}{\partial x^2} = -\frac{2mg}{\hbar^2}\left(\psi_0^2 - |\psi|^2\right)\psi, \tag{2.26}$$

which we can solve to give

$$\psi(x) = \psi_0 \tanh\left(\frac{x}{\xi}\right) \tag{2.27}$$

where ξ is the healing length, defined by

$$\xi = \frac{\hbar}{\sqrt{mgn_0}} = \frac{\hbar}{\sqrt{m\mu}}. \tag{2.28}$$

The healing length is a length scale which is the order of the distance from the boundary to the domain in which the density of the condensate is constant. For systems of higher chemical potential it is clear that the healing length is reduced due to higher energy interactions causing the condensate to spread out more.

2.5 Madelung Transformation

The relevance of the Gross-Pitaevskii equation to describing vortex dynamics can be made more transparent by re-arranging into a completely equivalent, but more fluid oriented, form by applying the Madelung transformation to equation (2.13). To apply the transformation consider the wavefunction in polar form, that is represented by a magnitude $\sqrt{n\left(\mathbf{r},t\right)}$ and phase $\theta\left(\mathbf{r},t\right)$;

$$\Psi\left(\mathbf{r},t\right) = \sqrt{n\left(\mathbf{r},t\right)}e^{i\theta(\mathbf{r},t)}. \tag{2.29}$$

The phase is linked to the fluid velocity. To find the fluid velocity we can use the momentum operator, $\hat{p} = -i\hbar\nabla$, far enough away from the boundary such that $n(\mathbf{r},t) = n_0$ where n_0 is constant. Then it follows that

$$\hat{p}\Psi(\mathbf{r},t) = -i\hbar\nabla\left(\sqrt{n_0}e^{i\theta(\mathbf{r},t)}\right) = \hbar\nabla\theta\left(\mathbf{r},t\right)\Psi(\mathbf{r},t) = p\Psi(\mathbf{r},t). \tag{2.30}$$

Thus the eigenvalue of the momentum operator is given by $p = \hbar\nabla\theta\left(\mathbf{r},t\right)$. Comparing this with the definition of momentum, $p = mv$, it is simple to see that

$$v = \frac{\hbar}{m}\nabla\theta. \tag{2.31}$$

Via substitution of the above representation of the wave function into the Gross-Pitaevskii equation and separation of real and complex terms, we arrive at two familiar equations. The equation found by consideration of the real part is the continuity equation,

$$\frac{\partial n}{\partial t} = -\nabla\cdot\left(nv\right). \tag{2.32}$$

This equation represents the conservation of number density withing the Gross-Pitaevskii equation and is equivalent to equation (2.15). The equation found by considering the imaginary parts is given by,

$$m\frac{\partial v}{\partial t} = -\nabla \cdot \left(\frac{1}{2}mv^2 + V_{ext} + ng - \frac{\hbar^2}{2m\sqrt{n}}\nabla^2\sqrt{n} \right). \tag{2.33}$$

This is very similar to Euler's equation (2.1) with a differing pressure term given by,

$$p = gn^2 - \frac{\hbar^2\sqrt{n}}{2m}\nabla^2\sqrt{n}, \tag{2.34}$$

known as the quantum pressure. The difference of the quantum pressure term is an important one, as the pressure is not constant the fluid will be compressible therefore the flow will host coherent structures such as sound waves and vortices. The second term in equation (2.34) is zero for a steady condensate with no external potential, whereas for a condensate confined to a potential at the boundary where $\nabla^2\sqrt{n}$ is non-zero this term becomes important at the boundaries and is associated with the healing length. As the wave function has been prescribed a flow velocity in equation (2.31), one can calculate the circulation. Substitution of (2.31) into the equation for circulation, (2.5), one will arrive at,

$$\Gamma = \frac{\hbar}{m}\oint_{\mathcal{L}} \nabla\theta \cdot d\mathcal{L} \tag{2.35}$$

Note here that if we let the value of Ψ at the beginning of the closed line integral to be Ψ_0 then at the end point of the line integral,Ψ_f, we obtain the expression $\Psi_f = \psi_0 e^{i\Gamma}$. However the wave function is single valued implying that $\Psi_f = \Psi_0$ thus Γ must be equal to some multiple of 2π. This is equivalent to,

$$\oint_{\mathcal{L}} \nabla\theta \cdot d\mathcal{L} = 2\pi q \tag{2.36}$$

where q is an integer. For a homogeneous condensate $q = 0$, however for $q \neq 0$ there must be a phase singularity in the flow. The phase singularity is present when considering the flow around a vortex. This causes the circulation to be quantized where q is the charge of the vortex. Substitution of equation (2.36) into equation (2.35) one will arrive at the circulation of a quantum fluid,

$$\Gamma = \frac{\hbar}{m}2\pi q = q\frac{h}{m}. \tag{2.37}$$

The circulation is quantized in units of h/m.

2.6 Sound Waves

The generation of sound waves within the condensate can be investigated by considering small perturbations to the wave function of the Gross-Pitaevskii equation. That is equivalent to applying the substitution $\Psi = \Psi_0 + \delta\Psi$ where Ψ_0 is the initial wave

function which is a solution to the time independent Gross-Pitaevskii equation and $\delta\Psi$ is a small perturbation from that state. Applying this to the one dimensional Gross-Pitaevskii equation, and removing terms of orders higher than $\delta\Psi$ to linearize, we find the expression,

$$i\hbar\frac{\partial}{\partial t}\left(\delta\Psi_0\right) = -\frac{\hbar^2}{2m}\frac{\partial^2}{\partial x^2}\left(\delta\Psi\right) + V_{ext}\delta\Psi + 2g\left|\Psi_0\right|^2\delta\Psi + g\Psi_0^2\delta\Psi^* \tag{2.38}$$

We proceed by considering solutions of the form

$$\Psi\left(x,t\right) = e^{-i\frac{\mu t}{\hbar}}\left[\psi\left(x\right) + u\left(x\right)e^{-i\omega t} + v^*\left(x\right)e^{i\omega t}\right], \tag{2.39}$$

where

$$\delta\Psi = e^{-i\frac{\mu t}{\hbar}}\left[u\left(x\right)e^{-i\omega t} + v^*\left(x\right)e^{i\omega t}\right], \tag{2.40}$$

correspond to small oscillations of the wave function around the ground state value. Substituting equation (2.39) into equation (2.38) and its complex conjugate, then proceeding by separating powers of the exponentials and noting that $\Psi_0\left(x,t\right) = e^{-i\mu t}\sqrt{n_0}$. Keeping only terms linear in u and v, we arrive at the coupled equations for the excitation amplitudes,

$$\left(-\frac{\hbar^2}{2m}\frac{\partial^2}{\partial x^2} + V_{ext} + 2gn_0 - \mu - \hbar\omega\right)u + gn_0 v = 0 \tag{2.41}$$

$$\left(-\frac{\hbar^2}{2m}\frac{\partial^2}{\partial x^2} + V_{ext} + 2gn_0 - \mu - \hbar\omega\right)v + gn_0 u = 0. \tag{2.42}$$

For a homogeneous system, where away from the boundaries $\mu = gn_0$ and $V_{ext} = 0$. We can consider plane wave excitations of the form

$$u\left(x\right) = u_0 e^{ikx} \tag{2.43}$$

$$v\left(x\right) = v_0 e^{ikx} \tag{2.44}$$

where k represents the wave number of the plane wave which then fixes ω as the angular frequency of the wave. Substituting the plane wave solutions into equations (2.41) and (2.42), we arrive at the equations

$$\left(\frac{\hbar^2 k^2}{2m} + gn_0 - \hbar\omega\right)u_0 + gn_0 v_0 = 0 \tag{2.45}$$

$$\left(\frac{\hbar^2 k^2}{2m} + gn_0 + \hbar\omega\right)v_0 + gn_0 u_0 = 0. \tag{2.46}$$

Solving these equations simultaneously and rearranging we find the relation:

$$\hbar^2\omega^2 = \frac{\hbar^2 k^2}{2m}\left(\frac{\hbar^2 k^2}{2m} + 2gn_0\right) \tag{2.47}$$

This is the dispersion relation for excitations in a homogeneous BEC. The speed of sound in the condensate will be the phase velocity of the excitation throughout the fluid. The phase velocity of a wave is given,

$$v_{phase} = \frac{\omega}{k}. \tag{2.48}$$

Rearranging equation (2.47) the speed of sound in the condensate can be given by,

$$c = v_{phase} = \frac{\omega}{k} = \sqrt{\left(\frac{\hbar^2 k^2}{4m^2} + \frac{g n_0}{m}\right)}. \tag{2.49}$$

Shortly after the realization of Bose-Einstein condensates, using the experimental methods discussed in the introduction, Wolfgang Ketterle [21] performed an experiment focused on sound waves. The experiment involved splitting a condensate using a laser then measuring how the energy propagated through the condensate. Figure 2.3 shows the results of this experiment, where 2.3a shows snapshots of the condensate at different times, one can clearly see there is a wave propagating through the medium and (2.3b) shows the results of changing the density and how this affects the speed of sound.

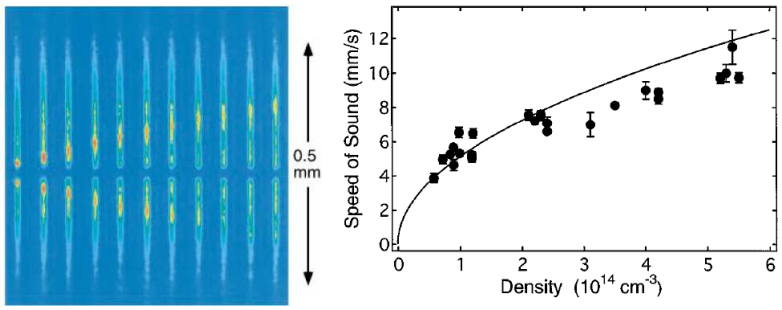

(a) (b)

Figure 2.3: Sound waves figures taken from [21]: (a) shows sound prorogation in a condensate taken using non-destructive phase imaging, this highlights the sound moving through the condensate; (b) shows how speed varies as a function of the initial density.

This experiment was performed on a BEC confined to a harmonic trap so the density was not homogeneous but a function of r in approximately one dimension. The perturbations were of a large wavelength so the speed in terms of density was approximately $c(r) = \sqrt{n(r)g/m}$. The wave number of the oscillations was comparable to the inverse healing length which is negligible when squared in equation (2.49).

Chapter 3

Numerical Methods

3.1 Dimensionless Gross-Pitaevskii

To make numerical simulations easier to implement, we shall use the dimensionless form of the Gross-Pitaevskii equation. A dimensionless equation is one in which the variables have all been scaled to dimensionless units. For the time dependent Gross-Pitaevskii equation the scales of choice are:

$$\begin{aligned} x &= \xi x' \\ t &= \frac{\hbar}{\mu} t' \\ \psi &= \psi_0 \psi' \\ V_{ext} &= V' \mu, \end{aligned} \tag{3.1}$$

where ξ is the healing length (2.28), μ the chemical potential and ψ_0 the solution to the steady infinite condensate. It then follows that the dimensionless Gross-Pitaevskii equation is given by,

$$i\frac{\partial \psi'}{\partial t} = -\frac{1}{2}\frac{\partial^2 \psi'}{\partial x^2} + V'\psi' + |\psi'|^2\psi' \tag{3.2}$$

which is the equation that is numerically simulated in this report. In order to see how to solve equation (3.2) numerically, let us first discuss some relevant background on numerical methods.

3.2 Finite Differences Method

Finite difference is a popular method for numerically calculating derivatives. The method relies on approximating derivatives at a particular point in space and time by considering nearby points at well defined finite distances. To begin we discretize our spacial domain, for one dimension this is x, into N_x points and temporal domain, t, into N_t points. The points are separated by small finite increments Δx and Δt for space and time

respectively. Within the scheme tho two important derivatives for solving the Gross-Pitaevskii equation are given by:

$$\frac{\partial\psi\left(x_j,t_p\right)}{\partial t}=\frac{\psi\left(x_j,t_p+\Delta t\right)-\psi\left(x_j,t_p-\Delta t\right)}{2\Delta t}+\mathcal{O}\left(\Delta t\right) \tag{3.3}$$

$$\frac{\partial^2\psi\left(x_j,t_p\right)}{\partial x^2}=\frac{\psi\left(x_j+\Delta x,t_p\right)-2\psi\left(x_j,t_p\right)+\psi\left(x_j-\Delta x,t_p\right)}{\Delta x^2}+\mathcal{O}\left(\Delta x^2\right) \tag{3.4}$$

where $\psi\left(x_j,t_p\right)$ is the approximation of the wave function at the point x_j at time t_p. The method also has a stability condition which is $\Delta t/(\Delta x^2)<1/2$. The error in the time step is of the order of Δt, this is not low enough to study dynamics in a reliable sense therefore it is necessary to implement a higher order time stepping scheme.

3.3 The Runge Kutta Method

The numerical method of choice for this report is the Runge-Kutta 4th order method because of its relative ease of use and its high stability. The method works by considering the approximate derivatives at different points and uses symmetry to cancel error terms from the approximations to increase the order of the truncation error. One could use a higher order Runge-Kutta method however the 4th order method is well within the required accuracy for the requirements of this report. The truncation error of the Runge-Kutta method is of the order of $\mathcal{O}\left(\Delta x^5\right)$ therefore the total error for multiple steps is of order $\mathcal{O}\left(\Delta x^4\right)$.

A simple algorithm can be implemented to choose optimum increments for numerical simulation. Firstly we choose the domain in which we want to study, that is defining x_{N_x} and x_1 so that $x_1\leq x_j\leq x_{N_x}$ for the discretized points x_j. We then choose the time frame in which we study and define it as so, $0\leq t_p\leq t_{N_t}$. These choices the determine the increments;

$$\Delta x=\frac{x_{N_x}-x_1}{N_x-1}, \tag{3.5}$$

$$\Delta t=\frac{t_{N_t}}{N_t}, \tag{3.6}$$

with N_x and N_t yet to be specified. The stability condition states that for stable solutions the increments must satisfy $\Delta t/(\Delta x^2)<1/2$, equivalently we can express this in terms of N_x and N_t and our chosen domains,

$$\frac{t_{N_t}/N_t}{\left(\left(x_{N_x}-x_0\right)/\left(N_x-1\right)\right)^2}<\frac{1}{2}\Rightarrow\frac{\left(N_x-1\right)^2}{N_t}<\frac{x_{N_x}-x_1}{2t_{N_t}}. \tag{3.7}$$

If we then set

$$N_t=\left(N_x-1\right)^2\frac{20t_{N_t}}{x_{N_x}-x_1} \tag{3.8}$$

we will be safely within the region of stability for any value of N_x. We can present this in the simplified example of the heat equation. The heat equation,

$$\frac{\partial u}{\partial t} = K\frac{\partial^2 u}{\partial x^2} \tag{3.9}$$

can be solved analytically. If we set constant $K = 1$ and specify the initial condition

$$u(x, 0) = \sin(\pi x) \tag{3.10}$$

for $0 \leq x \leq 1$ and choose the time we are interested in to be $t = 1$, the solutions is given by

$$u(x, t) = \sin(\pi x)e^{-\pi^2 t}. \tag{3.11}$$

Using the above algorithm with $x_0 = 0$, $x_{Nx} = 1$ and $t_{Nt} = 1$ we can solve the diffusion equation numerically and compare the results with the analytical solution for a variety of values of N_x and corresponding values of N_t by using the formula (3.8). Doing so we present the relative error, ϵ, in figure 3.1. From this figure we can see that in the region where $N_x > 300$ the increase in accuracy does not change much with increasing N_x. Increasing N_x is equivalent to an increase in computational time and as this is limited we must choose the smallest N_x such that we have adequate accuracy. We can repeat this process for solving the Gross-Pitaevskii equation in one and two dimensions.

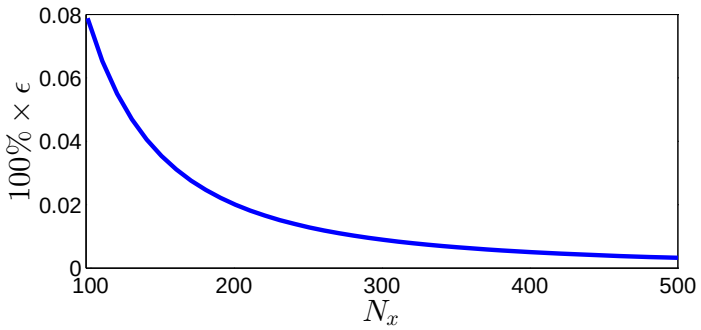

Figure 3.1: Relative Error: The plot of relative error, ϵ, as a percentage against increasing N_x which is equivalent to decreasing Δx.

3.4 Imaginary Time Propagation

To study the dynamics of the Gross-Pitaevskii equation in a controlled sense it is necessary to find the ground state. This state will be stable therefore perfect for studying controlled dynamics. A steady solution was found in section 2.4.2 for a homogeneous condensate however solutions for non-homogeneous condensates are not so simple. A good numerical method for calculating the ground state is Imaginary time propagation.

To gain insight into this method consider a wavefunction Ψ expressed as a superposition of eigenstates ψ_n with corresponding eigenenergies E_n given by

$$\Psi(x,t) = \sum_n a_n \psi_n(x)\, e^{-\frac{iE_n}{\hbar}t}. \tag{3.12}$$

In the above equation a_n are coefficients determined by the arbitrary state imposed. We can now order the eigenenergies with the condition that $E_n < E_{n+1}$, which implies that E_0 is the ground state energy. To proceed we consider the substitution $t = -i\tau$, which transforms the arbitrary state into the form

$$\Psi(x,\tau) = \sum_n a_n \psi_n(x)\, e^{-\frac{E_n}{\hbar}\tau}. \tag{3.13}$$

The above equation is decreasing in τ and will tend to zero as τ increases, this is unrealistic so we must impose a constant density by renormalizing. Renormalizing simply consists of calculating the initial density and rescaling the density on each iteration to that value. Equation (3.13) can be re-written, by taking the exponential of the lowest eigenenergy outside the sum, as

$$\Psi(x,\tau) = e^{-\frac{E_0}{\hbar}\tau}\left[a_0\psi_0 + a_1\psi_1(x)\, e^{\frac{(E_0-E_1)}{\hbar}\tau} + a_2\psi_2(x)\, e^{\frac{(E_0-E_2)}{\hbar}\tau} + \cdots\right]. \tag{3.14}$$

It is now clear that any term inside the bracket of the form,

$$a_n\psi_n(x)\, e^{\frac{(E_0-E_n)}{\hbar}\tau}, \tag{3.15}$$

will tend to zero as τ increases due to $(E_0 - E_n) < 0$ for $E_n > 0$. The speed of convergence to zero is increasing in n, thus the ground state will have the slowest convergence. This fact along with the renormalization imposing a constant density shows us that as τ increases Ψ will tend to the lowest energy state. By using the numerical methods discussed in the above sections with the substitution of $t_p = -i\tau_p$ we now have a method for finding the ground state. This method is also useful for the implementation of vortices. There is no exact analytical for for imposing a vortex into a condensate but there are many approximations. By using this method with the Gross-Pitaevskii equation we can implement a approximate vortex then reduce its energy to arrive at a better approximation for a steady vortex.

3.5 Ground State Solutions

Using imaginary time propagation as discussed in the previous section we arrive at a good approximation of an altered form of the analytical solution found in section 2.4.2. The form is altered to host the second potential wall defined by the box we are simulating. We created the new 'analytical' solution by overlaying the solutions to the two wall traps as if they were in each in a separate semi-infinite plane. We are able to do this as the

box we are simulating in has a much larger width than the healing length therefore the fluid at $x = -20$ is not interacting with the fluid close to the boundary at $x = 20$. The graphs are presented in figure 3.2.

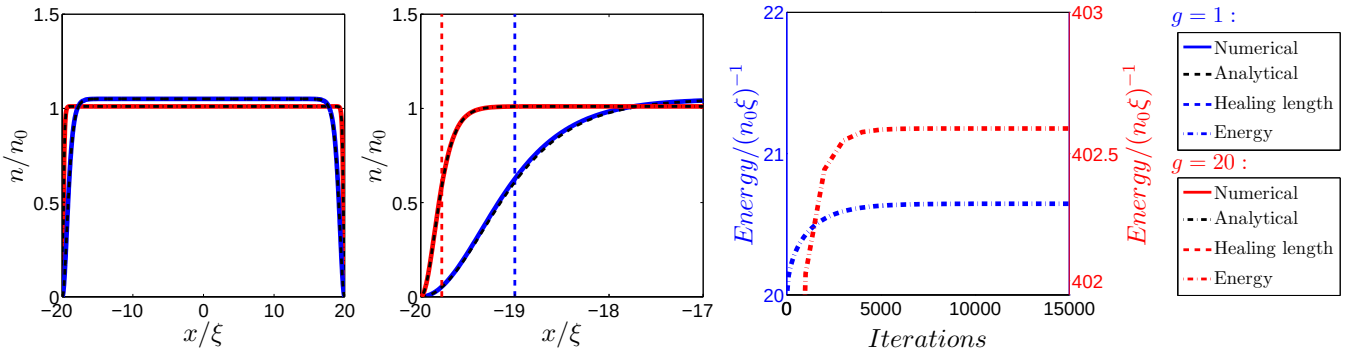

Figure 3.2: Ground state graphs: In these graphs the blue lines correspond to an interaction strength of 1 where the red lines represent an interaction strength of 20. The black lines are analytical solutions, where the dashed black line is the analytical solution when $g = 1$ and the dot-dashed line represents the analytical solution when $g = 20$. (b) represents a zoomed-in version of (a) and (c) is a graph of total energy against number of iterations in imaginary time, once again the blue line and left blue y-axis correspond to $g = 1$ and the red line and right red -axis correspond to $g = 20$.

Due to the rescaling of the Gross-Pitaevskii equation to dimensionless units the healing length now defines a unit of length for the case when the interaction strength is unity. 3.2b shows the effect of increasing the interaction strength. The most notice able change is the decrease in healing length, this change is expected and the direct magnitude of change can be found by considering (2.28). An intuitive explanation of this decrease can be found by studying the pressure term from the representation of the Gross-Pitaevskii equation found by applying the Madelung transformation. The pressure term, (2.34), away from the boundary is equal to gn^2 thus the pressure increases as g increases. The higher pressure is the cause of the healing lengths reduction. We can also see that as the two condensates have equal total density, the condensate with the larger healing length has a larger density away from the boundary. Figure 3.2c shows us that imaginary time propagation is working. After imposing an arbitrary superposition of states for our initial Ψ we can find the ground state energy.

3.6 Perturbations

Another valid check of our numerics can be made by considering the sound waves covered in section 2.6. In section 2.6 we saw that perturbations to the ground state of the Gross-Pitaevskii equation travel at a phase speed given by equation (2.48). Figure 3.3a

highlights this motions, we can see that after the initial ground state is perturbed sound waves propagate through the condensate.

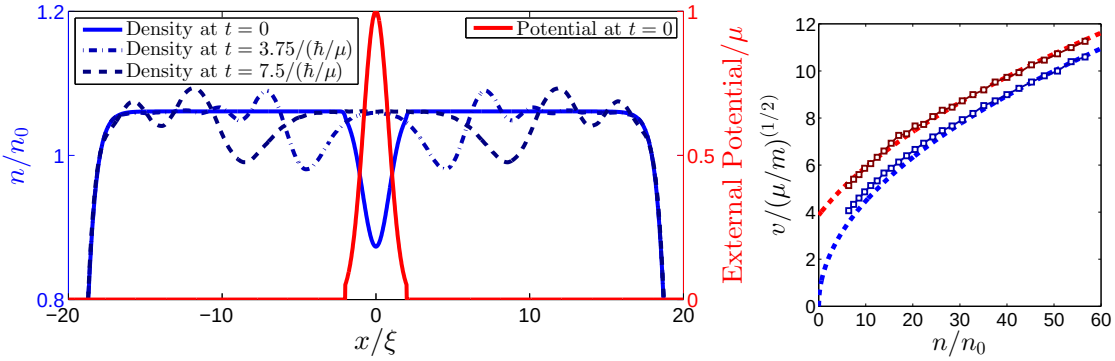

(a) (b)

Figure 3.3: Numerical sound waves: (a) shows sound propagating through the condensate as well as the potential which caused the perturbation. The red line and right axis corresponds to the potential. The blue lines correspond to the sound wave propagating through the condensate, The different line types of the blue lines correspond to different times as stated in the legend. (b) shows how the speed changes as a function of the background density. The blue data represent when the wave length is large ($\alpha = 0.001$) so the sound travels at $v = \sqrt{n'}$(which is the blue dashed line) and red line and markers represent when the sound has a shorter wavelength ($\alpha = 1000$) therefore traveling at a speed $v = \sqrt{k^2/4 + n'}$.

In figure 3.3a the potential used to create the perturbation is Gaussian and causes a perturbation in the form of a wave packet. The wavelength of the perturbation is larger if the wavelength of the potential used to perturb is larger. The direct relation is not trivial. To show the implications of equation (3.16) we can study perturbations of various wavelengths and calculate the phase speed of propagation of the perturbation. The results of such a study are presented in figure 3.3b. The potential applied in this study is the same as that in figure 3.3a. The potential is of the form $V = 0.25e^{-\alpha x^2}$. Where the value of alpha is changed for the two sets of values plotted. In this configuration where for the steady condensate with $V_{ext} = 0$ and away from the boundary and n_0 is constant the dispersion relation (2.47) will hold. The speed of a wave can be calculated using equation (2.49). Since the numerical simulations used a dimensionless Gross-Pitaevskii equation the speed measured will be given in dimensionless units. Applying the units (3.1) to the speed of sound, we arrive at the dimensionless formula

$$c' = \frac{\omega'}{k'} = \sqrt{\frac{k'^2}{4} + n'_0}, \tag{3.16}$$

which can be calculated via these numerics. By considering the position of the sound waves peak in figure 3.3a we can approximate the phase speed. Doing so we find the distance of the maximum points at $t = 3.75/(\hbar/\mu)$ and $t = 7.5/(\hbar/\mu)$ to be approximately

4.5ξ. This gives an approximate speed of $1.25/(\sqrt{\mu/m})$. Substitution of this into the formula for wave phase speed we can approximate the wavelength to be 4.4ξ which looks like a good estimate of the wave packets wavelength. We can investigate the spectrum of perturbations available in this system and study the different types of propagation. The smallest wavelength in this system will be of the order of the healing length where the largest will be twice the length of the condensate. The formula that relates the wavelength, λ, to the wave number k is simply $k = 2\pi/\lambda$. Using this formula we can calculate the corresponding wave number to the maximum and minimum wavelengths. The maximum possible wave number is given by $k_L = 2\pi/\xi$ whereas the minimum is $k_S = \pi/40$. The speeds of perturbations with wave numbers comparable to k_L are plotted in red in figure 3.3b whereas perturbations with wave numbers comparable to k_S are plotted in blue. The study undertaken in 3.3b is much like the numerical study undertook by Ketterle [21] discussed in section 2.6. We change the initial background density and show that the wave speed of a perturbation traveling through the condensate increases with the background density. We then go one further and vary the wave number. 3.3b shows the two similar cases to k_L and k_S and that the speed of the wave caused by the perturbation is dependent on its wave number.

Chapter 4

Dynamics of Two Vortices

We shall now present two different configurations of quantized vortex pairs. One is in which the pair are of equal and opposite circulation and the other with equal circulation with respect to both magnitude and direction. To start with we shall study the structure of both the vortex and antivortex.

4.1 Single Vortices

A single vortex in a homogeneous infinite system does not move without any other fluid motion such as boundary interactions or sound waves. This makes it an ideal building block for understanding the flow and structure of a quantized vortex.

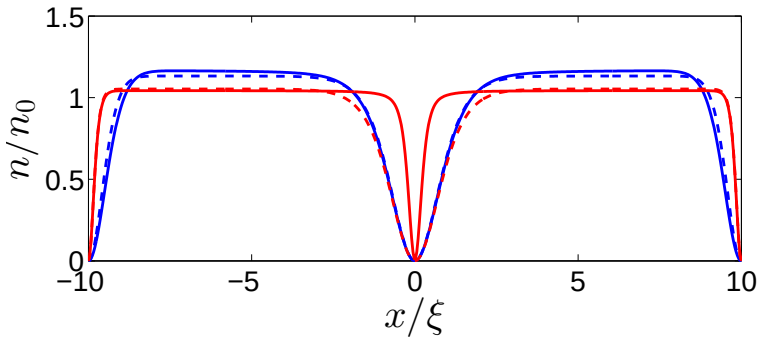

Figure 4.1: Vortex profiles: This figure is a slice of a two dimensional condensate on the line $y = 0$ with a vortex imprinted at the origin. The dashed line represents the vortex stamped in to the ground state condensate where the solid line is the condensate after propagation through imaginary time. The red lines corresponds to a condensate with $g = 20$ where blue lines correspond to an interaction strength of $g = 1$.

To create the vortex structure we find the steady state of a two dimensional condensate then multiply it by an approximation of a vortex core. The approximation of a

vortex whose center is at the coordinate (x_i, y_i) is of the form

$$\Psi_v = \Psi \prod_{i=1}^{N} \left(\frac{(x - x_i) \pm i(y - y_i)}{\sqrt{(x - x_i)^2 + (y - y_i)^2}} \right) \tanh(\sqrt{(x - x_i)^2 + (y - y_i)^2}). \tag{4.1}$$

where Ψ_v is the wave function with imprinted vortices, the plus imprints a vortex and a minus an antivortex. The blue and red dashed lines in figure 4.1 correspond to Ψ_v for a condensate with interaction strength 1 and 20 respectively. The approximations in figure 4.1 are not perfect thus to find the steady state we implement imaginary time propagation and arrive at the blue and red solid lines which are steady solutions. We can see that the core of the vortex is of the order of the healing length ξ. Although the vortex is stable in this configuration, moving the vortex from the origin will make the configuration unstable due to interactions with the boundary. Boundary interactions can be pictured as a vortex interacting with its mirror reflection with respect to the boundary. A single vortex against a boundary will act as a vortex-antivortex pair discussed in section 2.1.

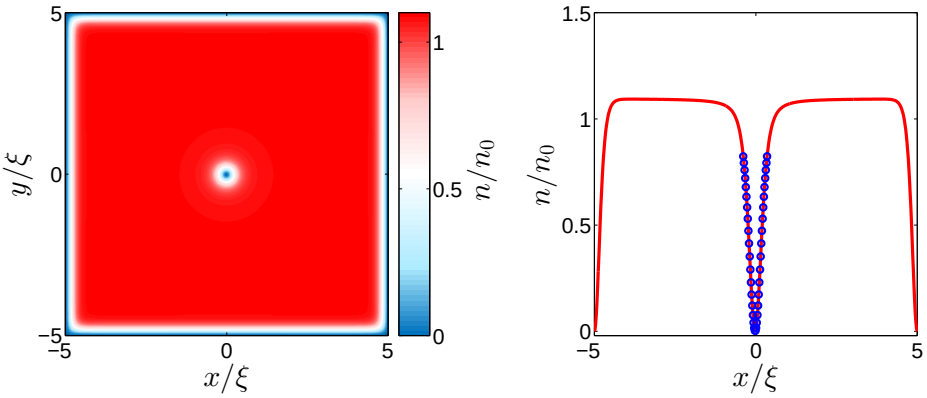

(a) (b)

Figure 4.2: Vortex graphs: (a) shows a contour plot in the x-y plane; In (b) the red line shows a slice of (a) where $|\psi(x, 0)|^2$ and the blue markers are points x_j on the numerical grid within the core.

From 4.2a we can see that the condensate has constant density everywhere except at the vortex and the boundaries due to the type of trap used. This is confirmed by 4.2b which shows the depth of the vortex in more detail. The blue points in 4.2b are the points of simulation within the vortex discussed in section 3.2, in this report a point within the vortex is defined to be at less than 85% of n_0 within a vortex region. It is important to have at least 15 points within a vortex when studying its dynamics to ensure the derivitive is a good approximation.

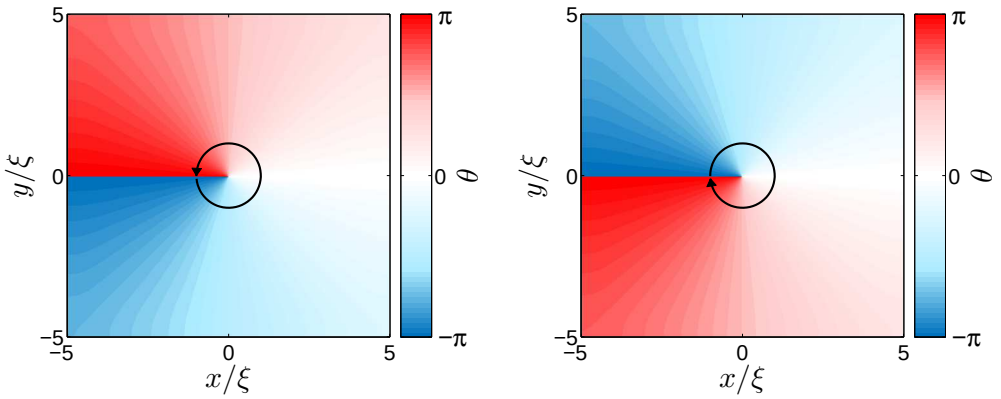

Figure 4.3: Vortex graphs: (a) shows the phase plot of a vortex; (b) shows the phase plot of a anti-vortex.

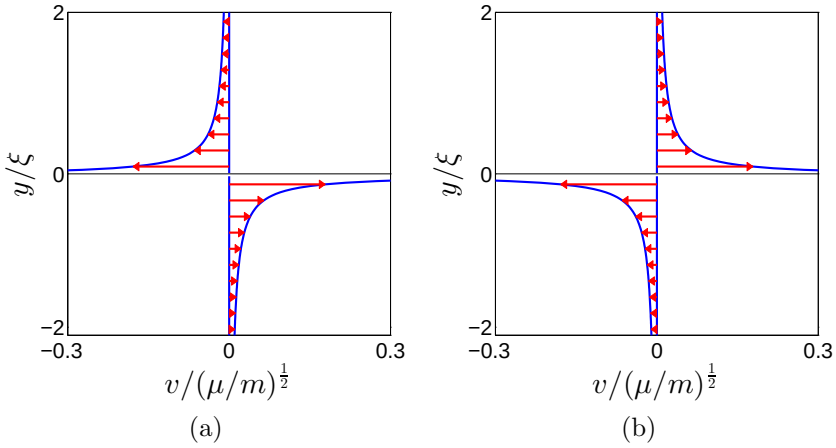

Figure 4.4: Velocity field graphs: Velocity of the flow on the y-axis of a vortex (a) and anti-vortex (b) positioned at the origin; The arrows are the velocity at a selection of points describing the magnitude via its length and direction via its direction. The blue line is represents the magnitude velocity field for all the points on the y-axis.

Figures 4.3a and 4.3b show the phase plots of a single vortex and a single anti-vortex, in the position shown by 4.2a, respectively. Using the phase plot it is easy to identify which one is a vortex and which is an anti-vortex. The convention is to define a vortex to have a positive phase change, i.e a positive flow (2.31), in an anti-clockwise direction. Figure 4.4 shows the velocity of the fluid on the y-axis of both a vortex and a anti-vortex. This also confirms that these vortices are in fact irrotational apart from at the singularity at the origin where the velocity field sharply falls to zero. For both graphs we can see that they are mirror images of one and other and that the definition depends on the observers position.
We can numerically compute a line integral around the vortex to check if the circulation

in this numerical model is in fact quantized, however first we will first have to calculate the dimensionless equation for circulation. To find the appropriate equation recall the scales used to make the Gross-Pitaevskii equation dimensionless (3.1). Applying these scales to the equation for circulation (2.5) and noting the units of velocity are $\xi\mu/\hbar$ simply derived from an arbitrary formula for speed. The dimensions of circulation will then be given by

$$\Gamma = \frac{\xi^2\mu}{m}\oint_{\mathcal{L}} \mathbf{v}' d\mathcal{L}' = \frac{\hbar}{m}\Gamma', \tag{4.2}$$

it is clear that the dimensions here are $\hbar/m$. Finally substitution into (2.37) gives that the dimensionless circulation will be $2\pi q$. By calculating a line integral around the vortices in an anti-clockwise direction, to coincide with convention, the circulation can be found to be 2π with a relative error of order 10^{-6} for the vortex and -2π with a relative error of 10^{-6} for the anti-vortex.
By calculating the energy of the ground state of a condensate then imprinting a vortex and calculating the energy we can calculate the energy stored in the vortex. Using this method we arrive at the vortex energy, $E_v \approx 0.46(\mu\xi n_0)$. The energy of the vortex will depend on its position within the condensate and also the interaction strength.

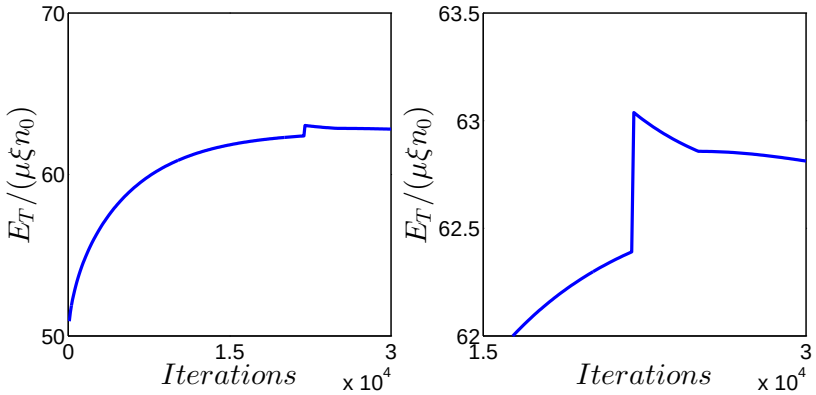

(a) (b)

Figure 4.5: Energy a Vortex: These graph show the total energy in the system for 30000 iterations. On the 20000^{th} iteration a vortex is imprinted into the system using equation (4.1). 4.5b is a zoomed in version of 4.5a. The Energy was calculated using the dimensionless from of equation 2.17.

We shall now introduce a second vortex to the system. The discussion will be separated into two sections, one section will cover the system containing two vortices of opposite sign also known as the vortex-antivortex pair, the other will cover the system of vortices with same sign known as the vortex-vortex pair. Firstly we shall study the structure of a general configuration of two vortices. Figure 4.6 shows two vortices imprinted in a condensate confined to a box spanning -5ξ to 5ξ in the x and y-directions.

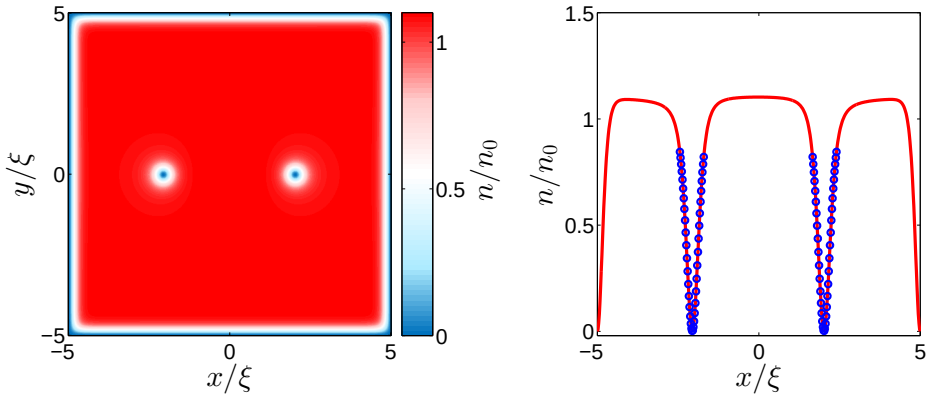

(a) (b)

Figure 4.6: Vortex - Vortex density graphs: (a) shows a contour plot in the x-y plane of two vortices, one positioned at (-2,0) and the other at (2,0). Figure (b) shows a slice of (a) in the x-$|\psi|^2$ plane where $y = 0$ the blue dots once again show the points within the vortices. The condensate here has interaction strength $g = 20$.

The density is zero everywhere except from at the boundary and the vortex cores. The density figure 4.6a and slice figure 4.6b are equivalent for both the vortex-antivortex pair and the vortex-vortex pair. We also see that the core size is identical to that of 4.2.

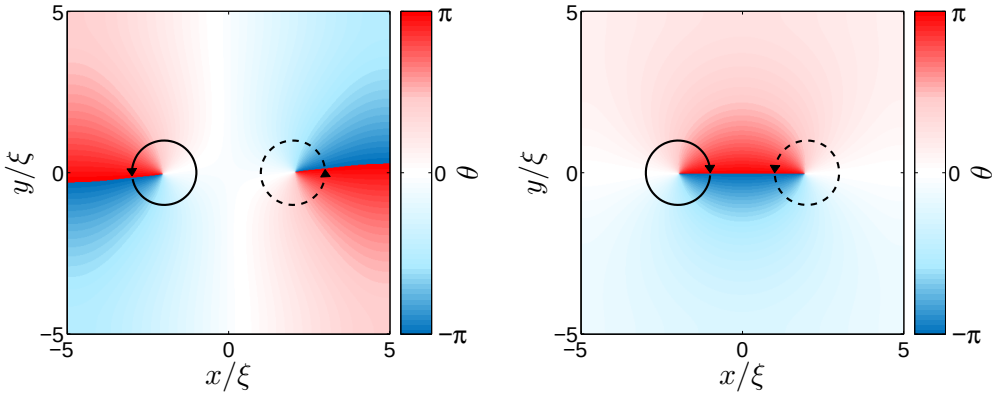

(a) (b)

Figure 4.7: Vortex - Vortex phase graphs: (a) shows the phase plot of the configuration of which the circulations are equal in magnitude but differ in direction; (b) shows the case in which the circulations are entirely in magnitude and directions. The black arrows indicate the direction of flow around each vortex.

Phase plots are useful for visualizing the velocity field of a fluid. By recalling the equation for the velocity of the flow (2.31), we can visualize the flow as moving from areas of low phase to areas of high phase as the arrows indicate. Using the arrows in the same way we studied the schematic, 2.1, we can predict the motion of the vortices. The initial motion of the vortex on the right in figure 4.7a will be in the positive

y- direction whereas the vortex on the left will be in the negative y-direction, this indicates that the vortices will rotate around one another in an anti-clockwise fashion. Both vortices' contribution to the velocity field push the opposing vortex in the negative y-direction in 4.7b, we can then predict parallel motion in this configuration. The circulation here is interesting because in the case of the pair with opposing directions of the circulation the overall circulation of the pair becomes zero to an error of 10^{-4}. The circulation in the case of completely equal circulation the circulation of the pair is close to 2π but off by a relative error of over 2%. From the phase plots in figure 4.6 we can see that the motions of the fluid are not as simple as for the single vortex pair, For this reason it will be neccesarry to procced by seperating the cases and studying the dynamics more rigorously.

4.2 Vortex-Antivortex Pairs

The vortex and anti-vortex are expected to follow parallel paths[1] as discussed in the previous section. As with the Euler point vortices we may expect the speed of the pair to be related to the distance between the vortex and antivortex forming the pair. To investigate the we simulated 16 different configurations of the vortex-antivortex pair with different separations. Due to the yet to be discussed annihilation when the vortex and antivortex's separation is close to the healing length not all the simulations were of use when investigating the speed. The results are presented in figure 4.8.

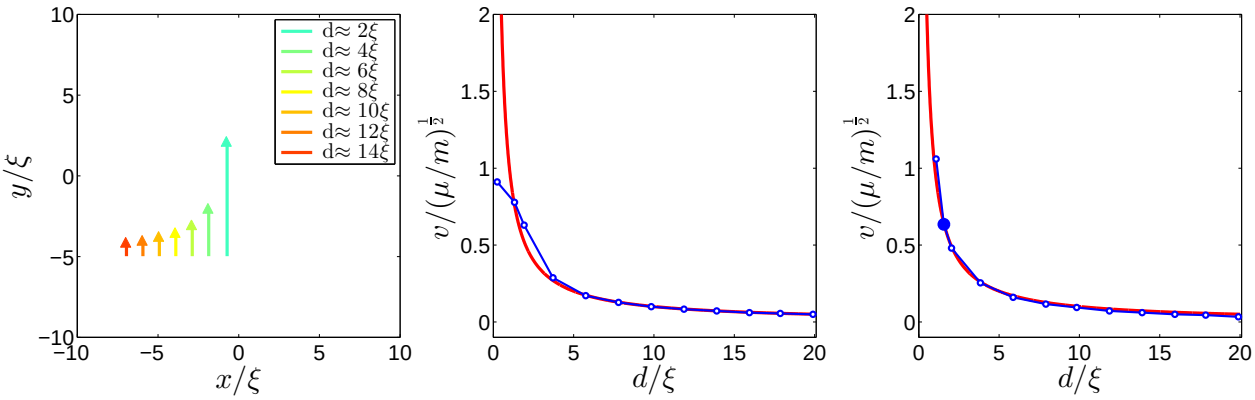

(a) (b) (c)

Figure 4.8: Vortex - Vortex graphs: (a) shows the paths of the vortex from the vortex-anti-vortex pair centered on $x = 0$ and $y = -5$ for 7 different initial separations d; (b) shows the speed as a function of the initial separation of the vortex and anti-vortex. The numerical results for the Gross-Pitaevskii equation marked with blue circles and connected by lines,the classical analytical equation, (2.7), is plotted in red; (c) is the same graph as (b) for vortices with smaller cores.

[1] A video of this motion can be found at [22]

From figure 4.8a it is clear that the speed of the vortex pair depends on the distance between them. In figure 4.8b we see that as the initial distance becomes larger between the vortices they tend to the dynamics of classical point vortices due to the core interactions becoming less important. This is highlighted in figure 4.8c when the core size is reduced the speed is very well approximated by classical point vortices. For further illustration of this motion we shall present a single example in more detail. The large filled point in figure 4.8c correspond to the example we shall illustrate. Density profiles and phase plots for a vortex-antivortex pair with a separation of $d = 4\xi$, which correspond to the large marker in figure 4.8c, are presented in figures 4.9 and 4.10.

The graphs in figure 4.9 show the emission of sound waves from the vortex-anti-vortex pair. One dimensional sound waves were discussed in section 3.6. Although the amount of energy released via the sound waves is small compared to the background density the fact that the emission occurs shows that this configuration is not stable in the stationary frame. The sound emission is associated with the acceleration of the vortices from zero velocity to the velocity in which the propagate through the condensate. Once the sound waves are moving at a constant speed they no longer emit sound. This is due to the vortex anti-vortex pair being a steady solution to the Gross-Pitaevskii equation in a moving frame. If the separation of the vortex anti-vortex pair is small enough the pair become unstable and annihilate[2]. The annihilation can be thought of the velocity fields canceling out as when the vortex and antivortex's centers are two close the contribution to the velocity field are in direct conflict. When the pair annihilates the energy contained in the pair forms radial sound waves. This energy is due to the energy associated with adding a vortex to the system as discussed for the case of the single vortex.

Using graphs 4.9e and 4.9f we can calculate the velocity of the sound wave and show that it is in accordance with the analytics. The minimum or trough of the sound wave is shown by the blue circle on both figures 4.9e and 4.9f. The top of the circle corresponding to the furthest distance the sound wave has traveled in the positive y-direction and is a good point to measure the speed. By considering the minima within regions of the snap shots of the condensate presented in figure 4.9e and 4.9f the approximate distance the wave has traveled can be found to be 13ξ. The time change between these figures is approximately $2.7\hbar/\mu$ which then implies the approximate phase speed of the wave is $c_a \approx 13/2.7 \approx 4.8$. Using this approximation of the sound along with the equation for phase velocity, (2.48), we can predict the wavelength of the sound emitted. Doing so we arrive at an approximate wavelength of 2.25ξ which from the figures looks reasonable and a further check made by considering the maxima at certain points was also in good agreement.

[2]A video of this occurring can be found at [23].

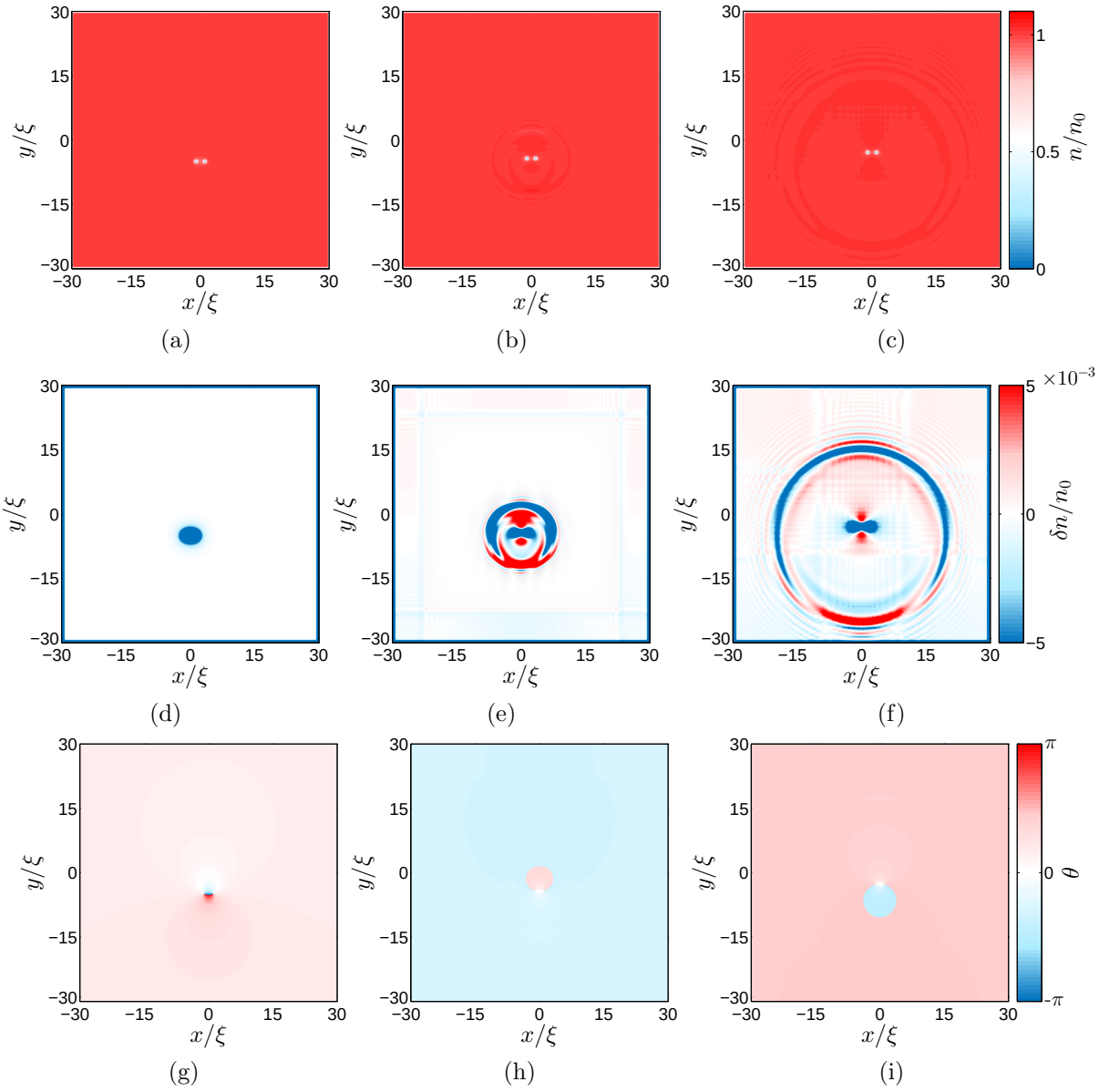

Figure 4.9: Vortex - Anti-Vortex graphs: (a),(b) and (c) show the density graphs at $t_0 = 0$,$t_1 \approx 1.5\hbar/\mu$ and $t_2 \approx 4.2\hbar/\mu$ respectively ;(d),(e) and (f) show the perturbations from the condensate at t_0, at t_1 and t_2;(g),(h) and (i) show the phase plots at t_0,t_1 and t_2.

By zooming in we can see the motion and structure of the pair in more detail. The small blue points in the top row of figures correspond to the center of the vortex. In the second row we can see that the pair actually form a dipole. The sound emission is symmetrical in the y-direction. We also see that there is no extra sound emission after the initial acceleration.

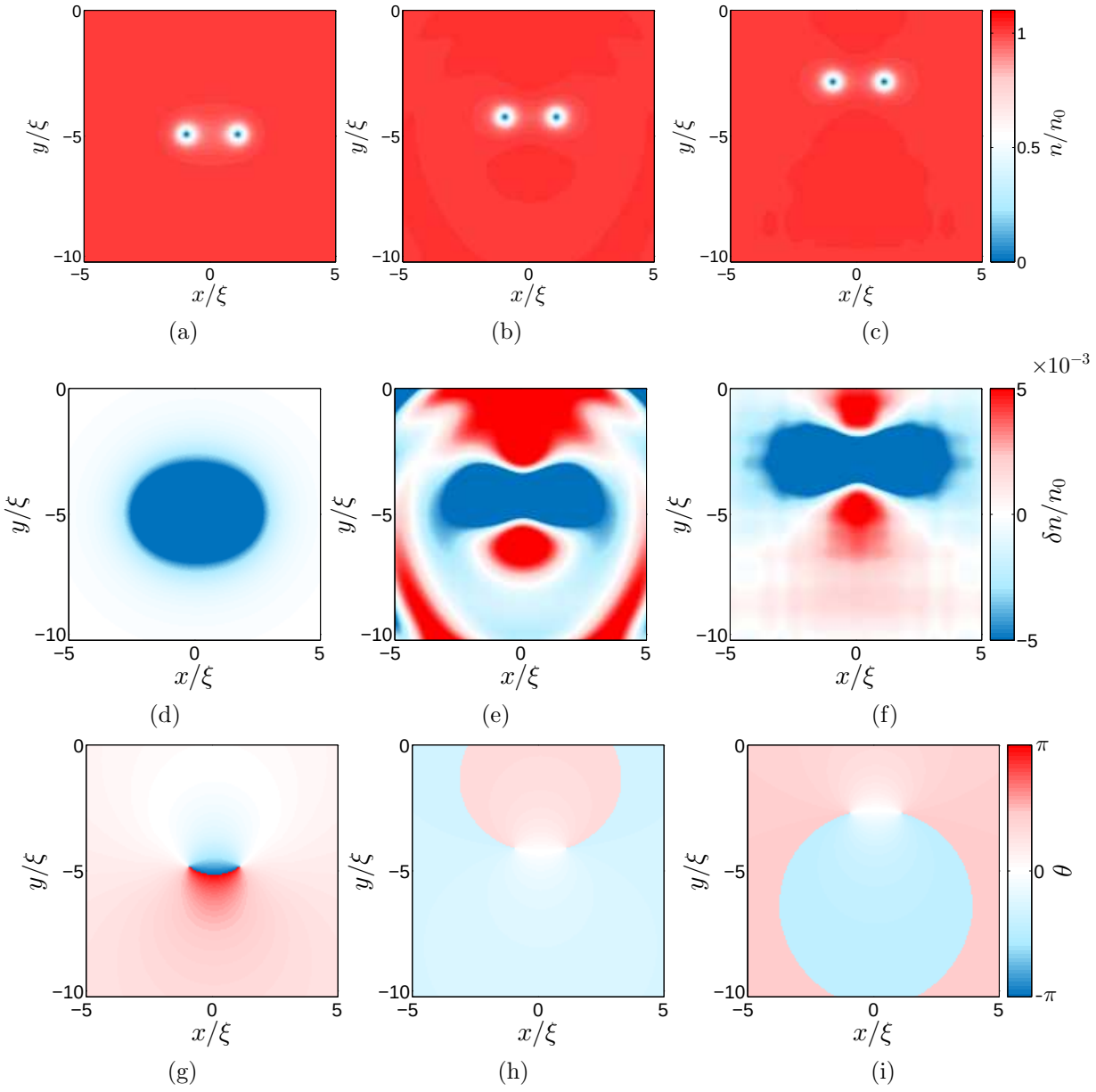

Figure 4.10: Vortex -antivortex zoom graphs: These graphs are the same as 4.9 however we have zoomed in on a small region showing the cores to clearly display the vortex-pair motions.

This can be seen in figure 4.10f as we would expect either red or blue circles radiating from the pair if there was any more sound emission. The change in colors in the bottom row of the above graphs shows the general flow of the fluid. The flow from low to high phase is always resulting in a positive flow from below the pair to above the pair. The line of separating high phase to low phase periodically interacts with the boundary. This is an example of the vortex being defined by the entire system it is contained in and not just the region of the core.

4.3 Vortex-Vortex Pairs

The focus of this section will be the configuration in which two vortices of equal circulation are printed into a condensate in a homogeneous trap at t_0. This configuration is the same as in the schematic (b). The box chosen has an area of $60\xi^2$ which spans from -30ξ to 30ξ in both the x and y direction.

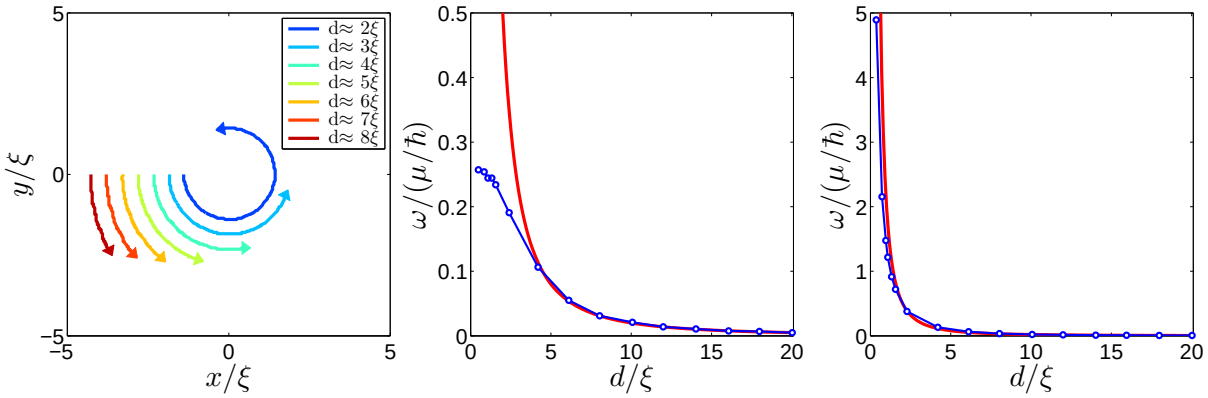

(a) (b) (c)

Figure 4.11: Vortex - Vortex graphs: (a) shows a selection the paths taken by the vortex whose starting position was $-d/2$. (b) shows how the angular velocity changes when the distance between vortices changes, numerical results (blue marked line), corresponding analytical result for classical vortices (red line) for 15 experiments. (c) is an equivalent graph to (b) with smaller cores.

From 4.11a the circular motion[3] of the vortices suggest that the configuration would be stable in a rotating frame; however, due to the acceleration involved in rotation being associated with sound emission it is not. 4.11b shows that the small core size used make the vortices act like infinitesimal Euler vortices. Although as the distance between the vortices becomes smaller the effect of the core makes the pressure term deviate from gn^2, the value which it takes for uniform parts of the condensate, and the second part of the pressure term becomes large. The stability of the pair can be investigated by looking at a particular point in more detail. The configuration we have chosen to discuss further is the one with the separation $d = 0.5\xi$.

[3]A video of this configuration can be found here [24]

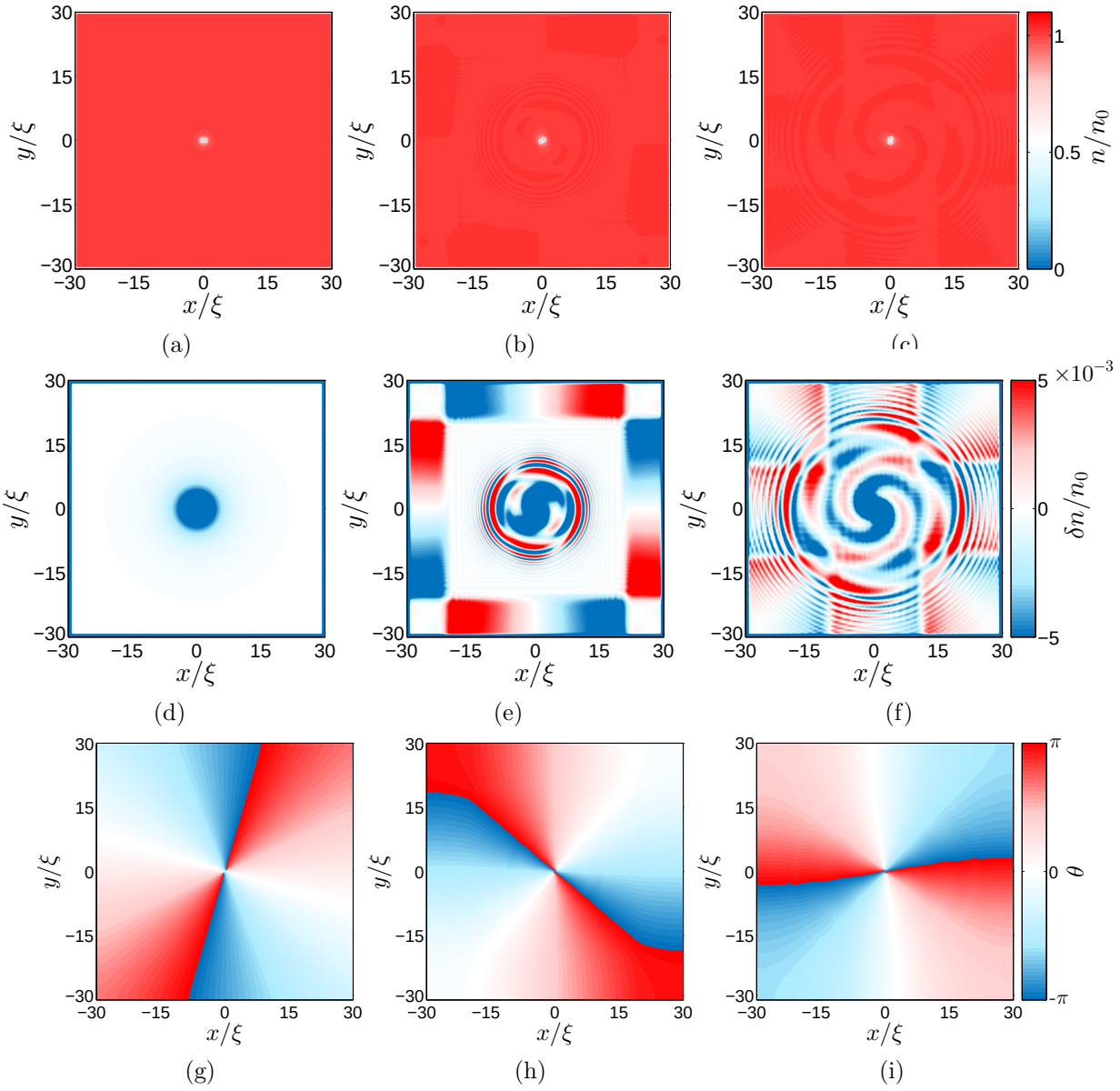

Figure 4.12: Vortex - Vortex graphs: (a),(b) and (c) show the density plots at $t_0 = 0$, $t_1 \approx 2\hbar/\mu$ and $t_2 \approx 4.2\hbar/\mu$ respectively, the plots highlight the rotational motion of the vortex pair. The small white dots correspond to the vortices.; (d),(e) and (f) show the sound emission on small density scales at t_0, t_1 and t_2 respectively. Here the initial configuration is unstable and emits sound energy. The sound energy then propagates outward toward the boundary; (g),(h) and (i) show the phase diagrams at t_0, t_1 and t_2 respectively.

The sound emission shown in the above figures differs from the case of parallel motion due to the constant acceleration associated with the angular velocity. Figure (f) captures the emission of sound from the pair which take the shape of a spiral. Once again the

sound energy emitted is small compared to the total energy of the system. Since there is sound energy constantly being emitted the configuration is not stable. The conservation of energy dictates that the vortex pair must separate to balance the energy lost. This separation happens slowly due to the small emission of sound.

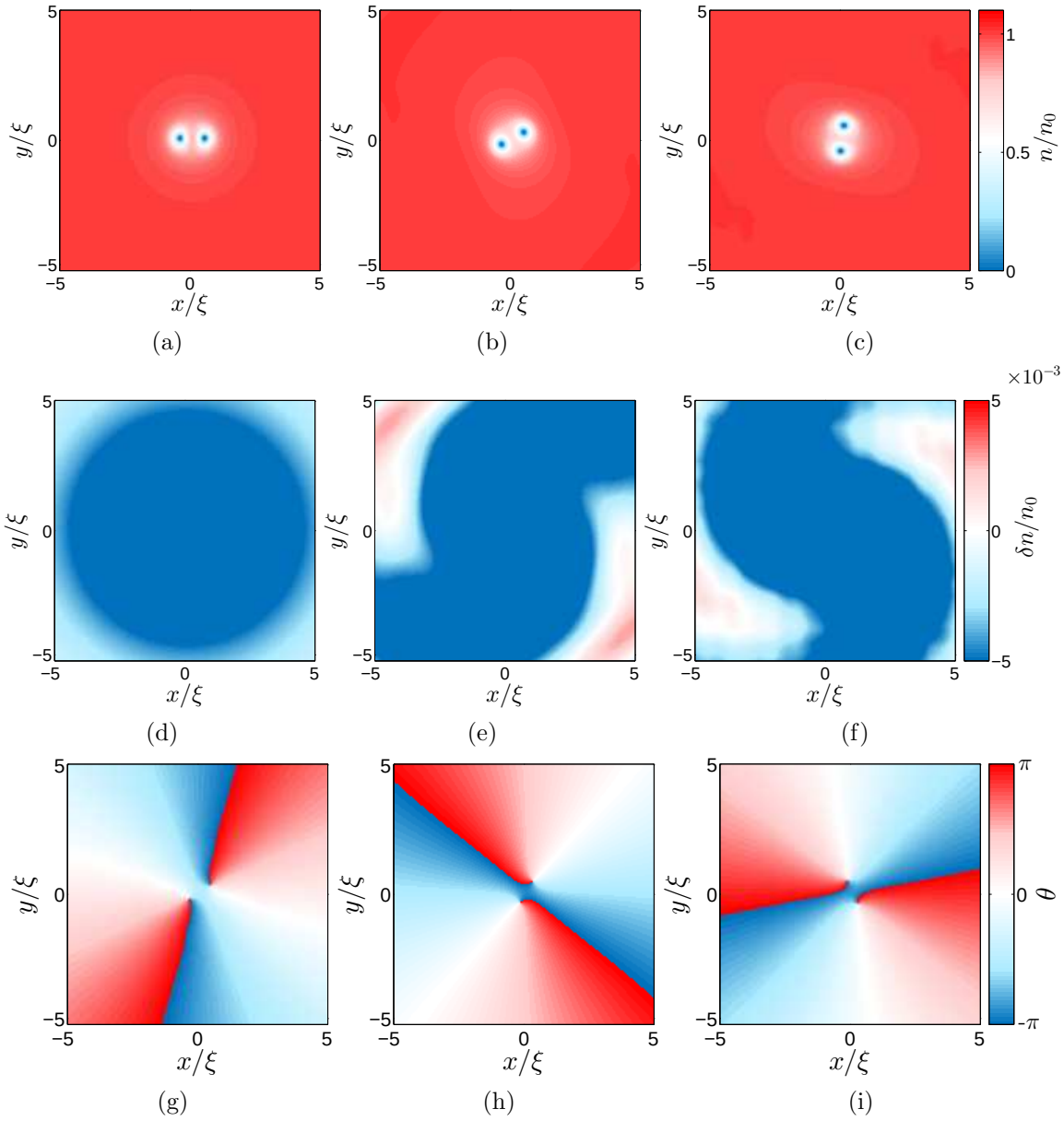

Figure 4.13: Vortex - Vortex zoom graphs: These graphs are zoomed-in versions of figure 4.12. The region presented spans from -5ξ t0 5ξ in both the y-direction and the x- direction. Each graph corresponds to the graph with the matching label in figure 4.12.

The top row of figures in 4.13 highlight the rotational motion of the vortex vor-

tex pair. The second row highlights the curvature of the sound waves being emitted from the pair. The final row is most insightful from these sets of figures. The figures show how the phase singularity wraps around the vortex. This causes the contribution to the velocity field of each vortex to push the opposing vortex away from it. To calculate the Energy in a vortex-vortex pair we can follow the same method as used to measure the energy of a single vortex. The method is to calculate the ground state energy via imaginary time propagation and then introduce a vortex-vortex pair. 4.14a shows the total energy of the system. As the system propagates through imaginary time the energy converges to the ground state energy E_0. On the 5000^{th} iteration we introduce a vortex-vortex pair, this is represented by the spike in energy in figures 4.14a and 4.14b. The system then propagates through imaginary time improving the approximation of the vortices we have implemented. As you can see the total energy E_T is larger that that of the ground state energy E_0, it then follows that the extra energy must be that of the vortex-vortex pair. We can then calculate the energy of the vortex vortex pair E_{vv} as $E_{vv} = E_T - E_0$. A plot of the energy of the vortex-vortex pair against the separation of the vortices is presented in 4.14c. E_{vv} decreases for larger separations, this is consistent with the energy stored in a classical Euler vortex vortex pair. Note that as the initial separation increases E_{vv} does not tend to zero as there is energy associated with the addition of single vortices. The repulsion of the cores along with the fact the energy stored in the pair decreasing when the separation increases causes the sound emission.

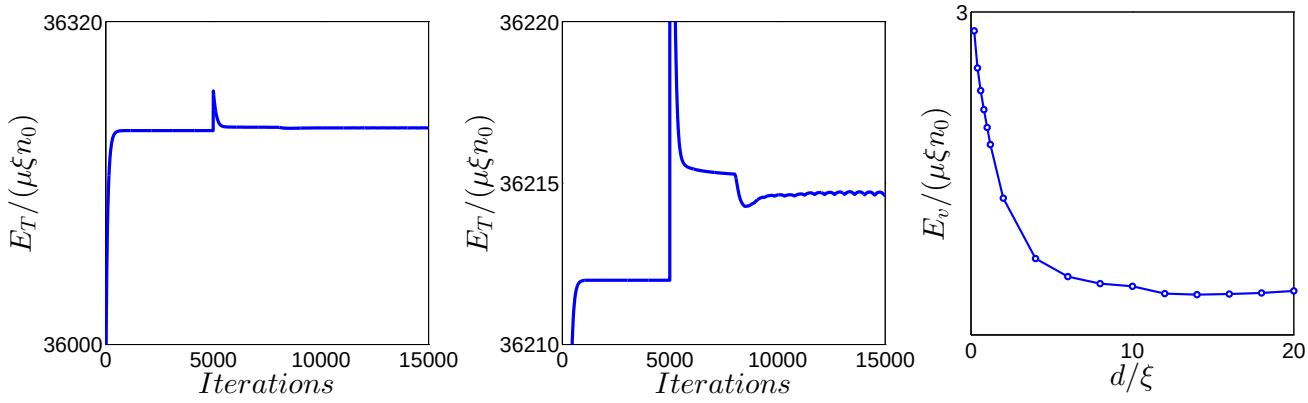

Figure 4.14: Energy of Vortex-vortex pairs: (a) shows the convergence of the energy of the condensate, on iteration 5000 a vortex-antivortex pair are introduced. (b) is the same graph as (a) but zoomed in and (c) is the energy the vortex-vortex pair adds to the system for 16 different separations.

Chapter 5

Dynamics of Three Vortices

There are a multitude of configurations to study containing three vortices all made more complicated by sound emission discussed in the previous sections of this chapter and chapter 3. Although the flows are not turbulent there is a great deal of complexity. The configuration this report is focused upon is that of a vortex pair interacting with a single vortex. An outline of the configuration is given in 5.1. The aim of the numerical experiment is to study if and how the impact parameter, h_0, and initial separation of the vortex-anti-vortex pair, d_0, affects the scattering angle θ.

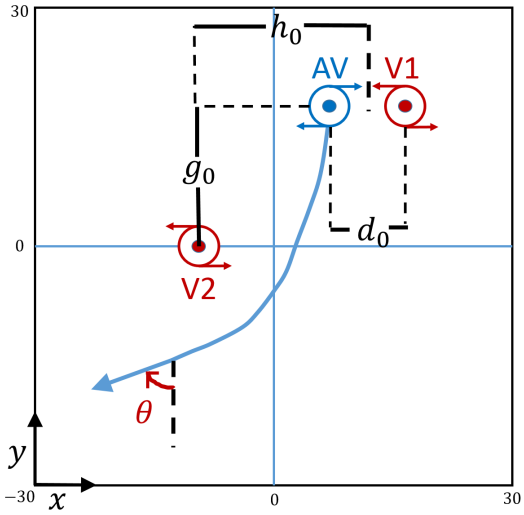

Figure 5.1: Outline of the numerical experiment: A vortex-antivortex pair (consisting of antivortex AV and vortex V1) is imprinted within a condensate as well as an additional vortex V2. The vortex-antivortex pair are configured so they have an initial motion solely in the negative y-direction. The antivortex, AV, is positioned a distance of $g_0\xi$ in the y-direction and a distance of the impact parameter $h_0\xi$ in the x-direction from the vortex V2. The final direction of the antivortex specified by the angle θ measured from the initial motion of AV is termed the 'Scattering' angle.

This configuration can be viewed as an approximation for a more complex three

dimensional configuration which would involve the interaction of two vortex rings. The vortex V2 would form a ring with its mirror image caused by the boundary at $x = -30$ as it is much closer to that boundary than the others. As the approximate consists of a small vortex ring we would not expect great accuracy.

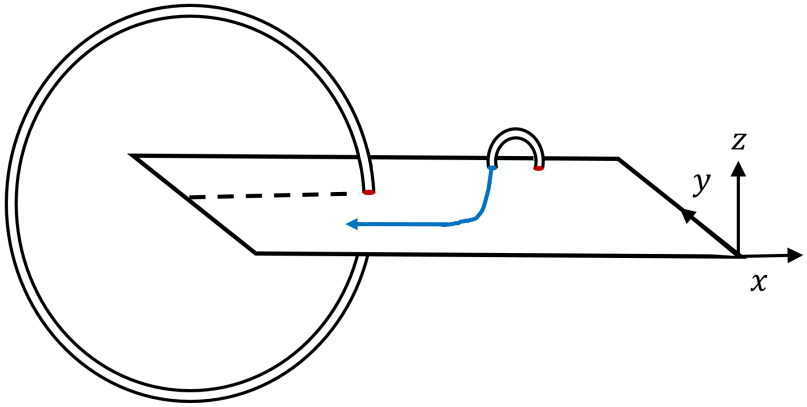

Figure 5.2: Vortex ring experiment: This figure shows how the 2 dimensional configuration can be seen as an approximate for a 3 dimensional system. The trapezoid shows a 2 dimensional box where intersections with the ring are vortex and antivortex cores shown as red and blue circles respectively. The vortex ring approximated by V2 and AV will move with a velocity v_p depending on the separation which is the equivalent to twice the radius of the vortex ring. The larger vortex's radius is large enough such that it has negligible motion and radius is the vortex V2's distance from the boundary.

5.1 Vortex Paths

To study the interactions of the three vortices we simulated the Gross-Pitaevskii equation for 16 different impact parameters spanning $h_0 = 5$ to $h_0 = 20$ for each of three initial distances. The initial distance's chosen are $d_0 = 3$, $d_0 = 4$ and $d_0 = 5$. There is a lot of data associated with that amount of simulation, for this report we are only focusing on the analysis of the paths. The paths were found by tracking each of the vortices cores motion. Some paths for the initial distances $d_0 = 4$ and $d_0 = 5$ are presented in figures 5.3 and 5.4 respectively. Due to imaginary time propagation minimizing the energy in the system the initial distances of the pair are altered through the process of stabilizing the initial configuration. We stabilize the initial configuration to reduce the effect of the sound emission on the results of the interaction. Because of the alteration of the initial distance the values for the impact parameters will be approximate.

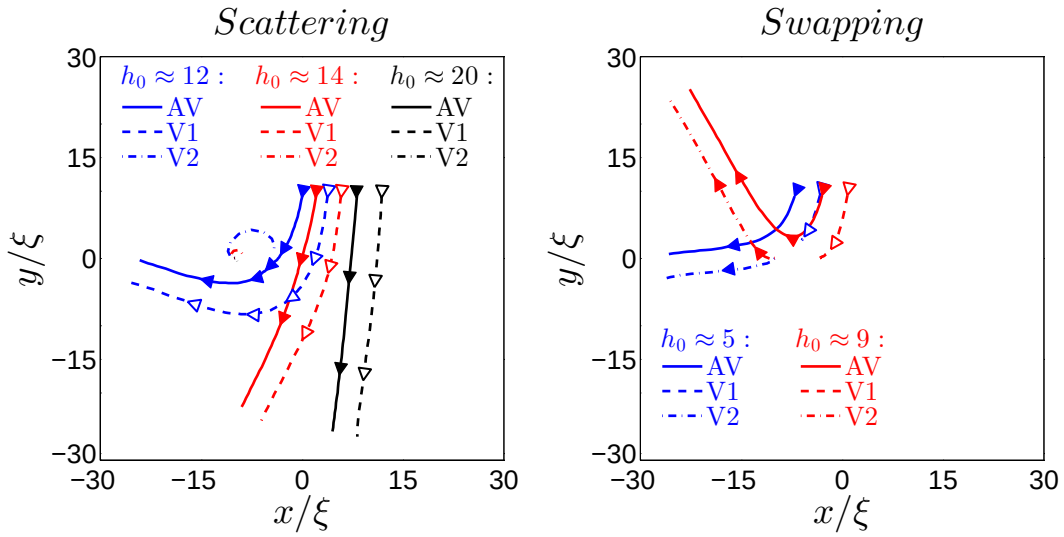

Figure 5.3: Vortex motion paths for initial separation $d_0 = 4$: (a) is the 'Scattering'[1]respectively. regime where the vortex-antivortex pair remain paired throughout the interaction. Each color represents a different isolated system. The solid line with filled arrows represents the anti-vortex, AV, and the dashed line with the empty arrows is the vortex, V1, which at $t = 0$ was in the vortex-antivortex pair. The dot-dashed line represents the motion of the vortex V2. (b) shows the 'Swapping'[1] regime where the anti-vortex, AV, forms a pair with the vortex which at $t = 0$ is in isolation. The definition of the line type are as before with the exception that vortex V1 with the dot-dashed red line's motion is represented by an empty arrow when it forms the pair.

As you can see in many of the simulations the antivortex is separates from its original parter V1 and forms a pair with vortex V2. The angle of motion of the new vortex pair in this regime is no longer a scattering angle. We proceed by separating the regimes and naming the regime where the vortex V1 is paired with the antivortex throughout the interaction the 'Scattering' regime and the regime where the antivortex switches affiliations the 'Swapping' regime. The figures indicate that the critical value of the impact parameter, we shall define to be h_{c_i}, differs for each value of d_0. The strength of the bond of the vortex-antivortex pair appears to increase as d_0 decreases, however; d_0 is bounded by a minimum value due to the annihilation discussed in section 4.2. This indicates there is a maximum possible bond of the pairing. Although the value of d_0 is also bounded above if as the vortex V2 would form a pair with AV if $d_0 > \sqrt{g_0^2 + (h_0 - d_0/2)^2}$, that is, the distance between AV and V1 becomes larger than the initial distance between V2 and AV.

[1]A video of the 'Scattering' and 'Swapping' regimes can be found at [25] and [26]

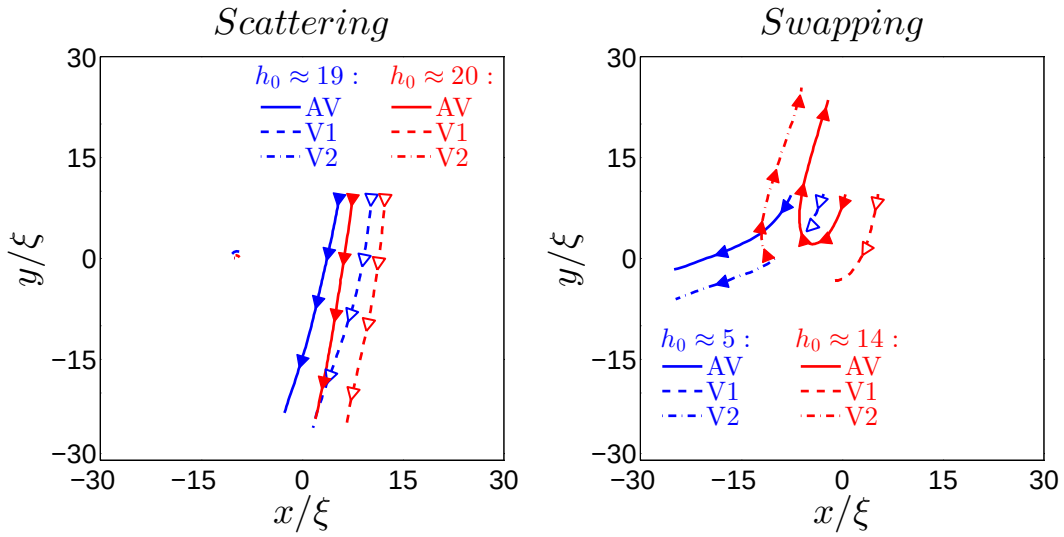

(a) (b)

Figure 5.4: Vortex motion paths for initial separation $d_0 = 5$: These graphs are the equivalent to 5.3 for the case of $d_0 = 5$

5.2 The Interaction

In this section we will analyze the interaction for both the 'Scattering' and 'Swapping' regime. The aim is to gain an understanding of the variables which are important for predicting the scattering angle θ. To begin we shall consider how the antivortex AV's speed changes throughout the interaction.

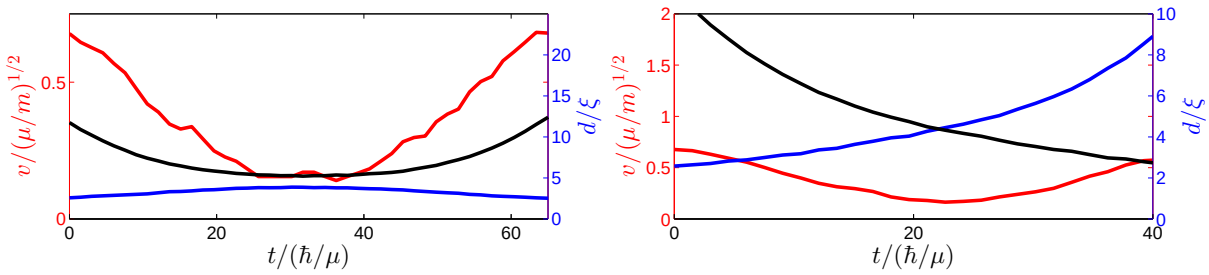

(a) (b)

Figure 5.5: Impact speed-distance for $h_0 \approx 5$ & $d_0 = 3$ and $h_0 \approx 4$ & $d_0 = 3$: The right axis corresponds to the blue and black lines which show the distance between the vortex V1 and anti-vortex AV, d_{V1} and the distance between antivortex AV and vortex V2, d_{V2} respectively. The left axis corresponds to the red line which represents the speed.

As we have seen the in section 4.2 the speed of a vortex-antivortex pair is directly related to the separation of the vortex and antivortex. Due to this dependence we specify the value d_{V1} to be the distance between the antivortex AV and the vortex V1

such that $d_{V1} = d_0$ at $t = 0$. As we have seen the antivortex forms a pairing with vortex V2 in the 'Swapping' regime, due to this it makes sense to also define d_{V2} to be the distance between the antivortex AV and vortex V2. Figure 5.5a is a plot of both these quantities and the speed of the antivortex throughout an interaction in the 'Scattering' regime and 5.5b represents an interaction within the 'Swapping' regime. Figure 5.5 shows that as the vortex-antivortex pair approach the vortex V1 the speed decreases with non-uniform deceleration. This hints toward a relation between the deceleration of the vortex pair and the distance from the vortex V1. The emission of sound energy is associated with the acceleration of a vortex core we expect to see ripples forming around the interaction area. Since this configuration is not stable in a stationary frame the initial sound produced interacts with its own reflections so the background density is dominated by sound therefore it makes viewing this emission considerably difficult.

The vortex-antivortex pair begin to separate as they approach vortex V2. The speed of the pair is still dependent on the separation between the vortex and antivortex; however, there appears to be a damping factor introduced by the the vortex V2. In both graphs the velocity of the antivortex AV hits its minimum when the ratio of d_{V2}/d_{V1} is at its minimum. The point when AV is moving at its lowest speed is when the interaction is at its peak. The difference in regime seems to be dependent purely on which vortex is closer to the anti vortex. To investigate this further we plot, for all simulations the ratio d_{V2}/d_{V1} against time.

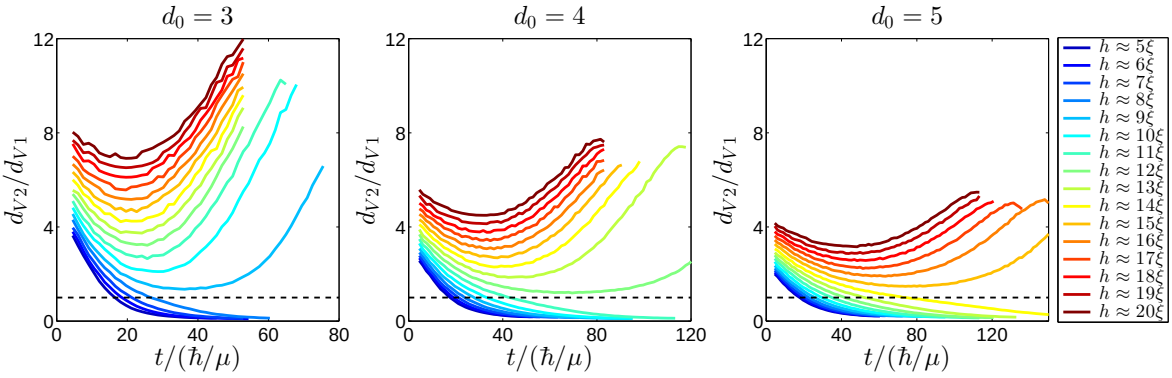

(a) (b) (c)

Figure 5.6: Ratios against time: The graphs show how the ratio d_{V2}/d_{V1} evolves in time. The evolution is plotted for each impact parameter separated by a different color, (a) represents the configurations in which $d_0 = 3$, (b) corresponds to $d_0 = 4$ and (c) to $d_0 = 5$. The black dashed horizontal line is the line $d_{V2}/d_{V1} = 1$.

In 5.6 we see that the ratio during the interactions become smaller for larger initial separations as expected. The line $d_{V2}/d_{V1} = 1$ specifies the difference between regimes. Any line that falls below the line, that is the antivortex AV becomes closer to V2 than

V1, is then part of the 'Swapping' regime. This is a clear indication that the ratio of distances d_{V1} and d_{V2} will be important in the model of the scattering angle.

5.3 The Scattering Angle

For each simulation we calculated the final direction of the antivortex and used this to calculate the angle θ. The scattering angles are presented for the 16 configurations with initial separation $d_0 = 4$ in figure 5.7.

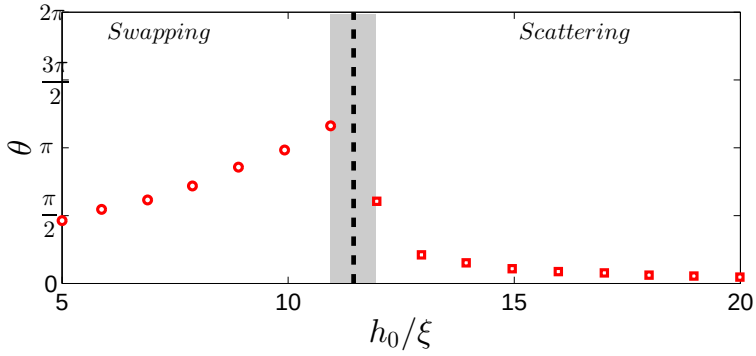

Figure 5.7: Different properties: This figure shows the discontinuity in the measured angles. Inside the shaded area is a region in which the true value of the critical impact parameter h_{c_4} lies. The swapping regime takes place within the region of the left of the shaded area and the change in the scattering angle within this regime is plotted as a circle. The scattering regime is present inside the region to the right of the shaded area and the angles are plotted as red squares. The black-dashed line here represents half way between the two experiments in between the regime changes, this value $h_c \approx 9.5$ is an estimate of the critical value.

As you can see it is appropriate to model the two different regimes separately as there is not enough data around the critical value to model the connection of the regimes. The critical value can be approximated by taking the midpoint of the two values for which the regime changes in between. We can speculate to the motion involved at the true critical value; however, more simulation would be required to say with any certainty. The first of the two possibilities that we suggest is that the vortex-antivortex pair fall into a fixed orbit around the single vortex. This would coincide with the model for the scattering regime tending to infinity as the impact parameter tends to the critical value. Another possible outcome is that an annihilation of the antivortex AV and V2 occurs.

The method for modeling the scattering angle, θ, as a function of h_0 and d_0 is to first consider the ratio d_{0_i}/h_0. This ratio is worth investigating as we have seen that the bond of a vortex-antivortex pair is related to the distance between the vortex and antivortex forming the pair. The ratio also satisfies one of the limiting cases, that is, as the impact parameter increases the scattering angle tends to zero. This is intuitive as when

the distance between the vortex-antivortex pair and the vortex V1 gets larger we would expect less of an interaction. However the ratio does not satisfy the second limiting case which is the case when the impact parameter approaches the critical impact parameter h_{c_i}. Although the outcome of this case is unknown to us we can use one of the ideas speculated earlier to create a model. The idea we will implement is the one where the pair fall into an orbit of the single vortex. This implies that the scattering angle will tend to infinity as the impact parameter tends to h_{c_i}. To introduce this limiting behavior into the ratio we can simply change the denominator to $h_0 - h_{c_i}$. We can also multiply by a free parameter, α, as it will not ruin the limiting behavior. Our model becomes

$$\theta = \frac{d_{0_i}}{4(h_0 - h_{c_i})}, \tag{5.1}$$

where $\alpha = 1/4$. The models along with the values calculated for the scattering angle are presented in figure 5.8.

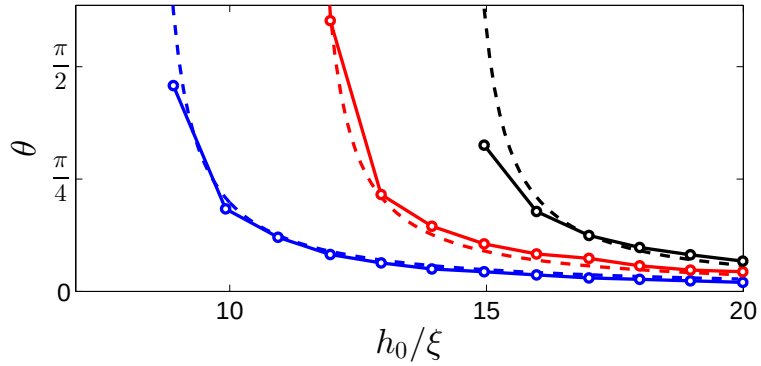

Figure 5.8: Impact angle as a function of the impact parameter h_0 and initial separation d_0: This shows the model for the 'scattering' regime which the model (dashed line) is $\theta_i = d_{0_i}/4(h_0 - h_{c_i})$.

The above figure shows that the model for θ is a good fit. The model depends on the critical value, which for $d_0 = 5$ the guess of the critical value, made by taking the midpoint of the values at which the regimes change, seems to be poor in comparison to the other two models. We could improve the model by more simulation around the critical value or improve the method we use to guess the critical value. The model also depends on the free parameter $\alpha = 1/4$. To improve the model we could investigate the free parameter.

We expect another regime change when the impact parameter decreases and the pair no longer interact with the vortex V2. This regime will be much like the 'Scattering' regime however the interaction will be different due to the vortex-vortex interaction being the interaction of interest in this scheme. Due to this unknown regime and no way of approximating the critical value at which the regime changes we are unable to create a model for the 'Swapping' regime; however, we present the values of θ calculated to show there is a trend followed by the points and this regime is worth investigating further.

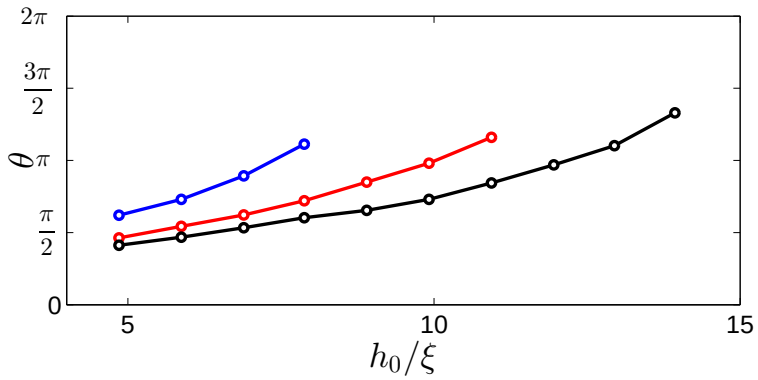

Figure 5.9: Results for the simulations in the 'Swapping' Regime: The points represent the scattering angle connected by a line to show the relation.

There appears to be limiting behavior as the impact parameter reduces; however, we do not have enough evidence to suggest a particular value. The values show that the scattering angle in this regime is also effected by the initial distance separating the vortex-antivortex pair. To create a complete model for the scattering angle we suggest a further study where we increase the domain in which we study the impact parameter as well as a smaller increment between the impact parameters at points of interest such as at the critical values.

Chapter 6

Conclusion & Further Work

We have undergone a numerical study for the 'quantum' vortex via simulation of the Gross-Pitaevskii equation. In this report we have studied the structure of the quantum vortex in a homogeneous system. After studying the discussing the relevant features of the single 'quantum' vortex we studied the system configured of multiple systems. Initially we discussed the interactions of the vortex-vortex pair and the vortex-antivortex pair then we moved onto an interesting interaction of three vortices. Whilst studying the configuration of two vortices we focused on the speed of the vortex pairs and the emission of energy via sound waves and noted that it was an indication of the stability of the configuration. This study of two vortices became useful when investigating the configuration of three vortices in a manner in which we were not able to find any relevant publication. We determined a good model for the scattering angle of a vortex-antivortex pair incident on a single vortex based on a critical value and free parameter which themselves require more study. We also discussed another interaction which we labeled the 'Swapping' regime. In this regime we were not able to create a presentable model for the data due to the lack of study on the limiting cases. This sets up nicely for further study in this topic.

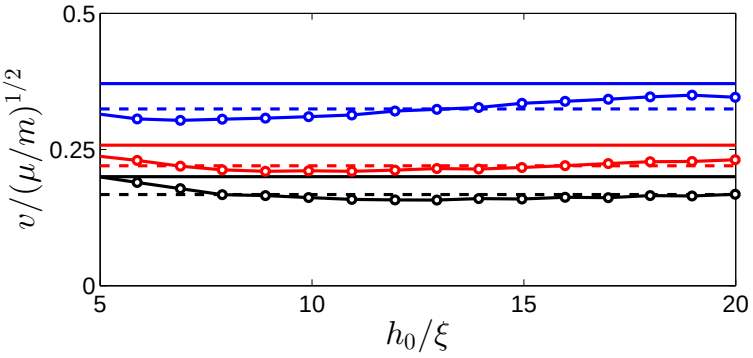

Figure 6.1: Initials speeds: This graph shows the initial speeds of the vortex-antivortex pair for the numerical experiment. The dashed lines represent the mean values for the initial speeds. The blue line corresponds to $d_0 = 3$, the red $d_0 = 4$ and the black $d_0 = 5$. The solid line correspond to the speed calculated using the classical approximation 2.7.

The results obtained in the final section of this report are preliminary. As outlined there are improvements to be made to the numerical experiment, such as implementing larger initial distances and reducing the effect of boundary interactions. Figure 5.7 shows the initial speeds as well as the approximate speed using the classical model which we showed was a good approximation for separations considerably larger than the vortex core. The figure shows the distribution of initial speed, in an ideal numerical experiment the points would be at a constant speed for all impact parameters; however, due to lack of computational power and time we had to simulate in a box of limited size. This resulted in an initial configuration where the vortex-antivortex pair were already interacting with the vortex. To remove this interaction the simulations can be repeated with a larger g_0.

After making the numerical improvements and comparing the results to the ones found we can increase the amount of data and check the fit of the proposed models for the scattering angle. The interaction close the the critical value plays an important role and further study developing the understanding of the variables which determine the critical value is needed. The emission of sound during the interaction will be of importance to the outcome of the interaction. To study the emission of sound we would have to simulate in a box in which the boundary is at a distance further than the sound can travel during the time it takes for the interaction to complete. The size of this box is considerably large and require heavy numerics; however, this would make an interesting study and may also contribute to parameters not mentioned in this study such as the finial separation of the vortex-antivortex pair and its speed.

The study presented in this report highlights the complex motion involved in the interaction of three quantum vortices. Although the results are preliminary they show that in the case of three vortex interaction, within the Gross-Pitaevskii model, there is an ability to characterize the interaction via the scattering angle. We can continue to characterize the other three vortex in the same manner as the interaction presented in the report. The other vortex motions can be found by differing the initial configuration of the vortices and also changing the amount of vortices and antivortices.

Bibliography

[1] T. Meuel, Y. L. Xiong, P. Fischer, C. H. Bruneau, M. Bessafi, and H. Kellay., "Intensity of vortices: from soap bubbles to hurricanes.," *Scientific Reports*, vol. 3, no. 3455, pp. 1–7, 2013.

[2] H. Suwa, Y. Suzuki, and A. Yokoo, "Estimation of exit velocity of volcanic plume from analysis of vortex structures," *Earth and Planetary Science Letters*, vol. 385, p. 154161, 2014.

[3] C. P. Ellington, C. van den Berg, A. P. Willmott, and L. R. Thomas, "Leading edge vortices in insect flight," *Nature*, vol. 384, no. 19, pp. 626–630, 1996.

[4] G. Pedrizzetti, G. L. Canna, O. Alfieri, and G. Tonti, "The vortex–an early predictor of cardiovascular outcome?," *Nature Review Cardiology*, vol. 11, no. 9, pp. 545–553, 2014.

[5] P. G. Saffman and G. Baker, "Vortex interactions," *Ann. Rev Fluid Mech.*, vol. 11, no. 1, pp. 95–121, 1979.

[6] M. H. Anderson, J. R. Ensher, M. R. Matthews, C. E. Wieman, and E. A.Cornell, "Observation of Bose-Einstein condensation in a dilute atomic vapor," *Science*, vol. 269, no. –, pp. 198–201, 1995.

[7] K. B. Davis, M. O.Mewes, M. R. Andrews, N. J. van Druten, D. S. Durfee, D. M. Kurn, and W. Ketterle, "Bose-Einstein condensation in a gas of sodium atoms," *Physical Review Letters*, vol. 75, no. 33, pp. 3969–3973, 1995.

[8] L. Onsager, "Statistical hydrodynamics," *Nuovo Cimento*, vol. 6, no. 2, p. 281, 1949.

[9] R. J. Donnelly, *Quantize Vortices in Helium II.* –: Cambridge Studies in Low Tempurature Physics, 1991.

[10] R. P. Feynman, "Application of quantum mechanics to liquid helium.," *Progress in low temperature physics*, vol. 1, no. 1, pp. 17–53, 1955.

[11] H. E. Hall and W. F. Vinen, "The theory of mutual friction in uniformly rotating helium ii," *Royal Society*, vol. –, no. II, pp. 215–234, 1956.

[12] M. R. Matthews, B. P. Anderson*, P. C. Haljan, D. S. Hall, C. E. Wieman, and E. A. Cornell*, "Vortices in a Bose-Einstein condensate," *Physical Review Letters*, vol. 83, no. 13, pp. 2498–2501, 1999.

[13] J. R. Abo-Shaeer, C. Raman, J. M. Vogels, and W. Ketterle, "Observation of vortex lattices in Bose-Einstein condensates," *Science*, vol. 292, pp. 476–479, 2001.

[14] T. W. Neely, E. C. Samson, A. S. Bradley, M. J. Davis, and B. P. Anderson, "Observation of vortex dipoles in an oblate Bose-Einstein condensate," *Physical Review Letters*, vol. 104, no. 16, pp. 1–4, 2010.

[15] H. Aref and N.Pomphrey, "Integrable and chaotic motions of four vortices," *Physics Letters*, vol. 78A, no. 4, pp. 297–300, 1980.

[16] N. Parker, "Numerical studies of vortices and dark solitons in atomic Bose-Einstein condensates," *PhD thesis, Durham University*, vol. Chapter 8, p. 137151, 2004.

[17] B. Damski and K. Sacha, "Changes of the topological charge of vortices," 2002.

[18] E. P. Gross, "Structure of a quantized vortex in Boson systems," *NUOVO CIMENTO*, vol. XX, no. 3, pp. 454–477, 1961.

[19] L. P. Pitaevskii, "Vortex lines in an imperfect Bose gas," *Soviet Physics JETP*, vol. 13, no. 2, pp. 451–454, 1961.

[20] L. Pitaevskii and S. Stringari, *Bose-Einstein Condensation*. –: Oxford Science Publications, 2003.

[21] M. R. Andrews, D. M. Kurn, H.-J. Miesner, D. S. Durfee, C. G. Townsend, S. Inouye, and W. Ketterle, "Propagation of sound in a Bose-Einstein condensate," *Physical Review Letters*, vol. 79, no. 4, pp. 553–556, 1997.

[22] A. Griffin, "Youtube: Vortex-anti-vortex pair.." Link: `https://www.youtube.com/watch?v=D7oBEGqudGU`. url date: 2015-04-19.

[23] A. Griffin, "Youtube: Vortex-anti-vortex pair annihilation.." Link: `https://www.youtube.com/watch?v=VPADTbNGsDE`. url date: 2015-04-19.

[24] A. Griffin, "Youtube: Vortex-vortex pair.." Link: `https://www.youtube.com/watch?v=otoRAuLXbIc`. url date: 2015-04-19.

[25] A. Griffin, "Youtube: Scattering of vortex-anti-vortex pair.." Link: `https://www.youtube.com/watch?v=WzvmVMwcH2Y`. url date: 2015-04-19.

[26] A. Griffin, "Youtube: Vortex-anti-vortex swap.." Link: `https://www.youtube.com/watch?v=JYtcb77Wynk`. url date: 2015-04-19.